Fabrication and Characterization of Nano Aperture Ion Source For High Brightness Proton Beam Writing

Pang Rudy

A0081188Y

National University of Singapore

Supervisor: A/Prof Jeroen Anton van Kan

Co-Supervisor: Asst Prof Slaven Garaj

A thesis submitted in partial fulfilment for the degree of

Bachelor of Science (Honours) in Physics

2015 April

Abstract

Current microelectronics production are only capable of producing two-dimensional micro-structures in integrated circuits and the next huge step forward is the production of 3D structures for better and smaller devices. Thus, in this project, we are using MEMS fabrication techniques to develop a high brightness proton beam writing system which is capable of directly writing high aspect ratio 3D micro- and nano-structures.

In this report, we modified and fabricated an electron gas impact ion source, which relies on the extraction of positively charged ions from a gas chamber where neutral gas atoms become ionized using direct electron impact. We estimated that using a small gas chamber, the reduced brightness of this source can exceed that of the current radio-frequency(RF) source. To proof the concept, testing of the ion source was done with the ion beam giving a current density of 42.4 A/m^2 which is approximately 100 times more than the current density of the 2nd generation proton beam writer.

To continue the test for the ion source, an aperture is required to focus the beam as well as to use the double aperture opening to calculate the reduced brightness. Currently, the aperture is in the final phase of development, but measurements of the aperture shows the fabricated windows being much larger than intended. The reason was discovered to be due to the much thinner silicon wafer measured to be 492μm as the thickness of the silicon wafer used as back-calculations of the aperture sizes were done using the stated 525μm. Experiments to test the apertures are still expected to continue even with the setbacks.

Acknowledgements

First and foremost, I would like to express my deepest appreciation to my Supervisors, Professor Jeroen and Professor Slaven for giving me the opportunity to do my final year project in the field that I am interested in. I am greatly indebted to Professor Jeroen for his guidance and supervision as well as for providing the necessary information regarding the project as without his help, this project would not have been possible.

I would also like to express my gratitude to my fellow colleagues, Liu Nannan, Xu Xinxin and Dr Raman for their continuous guidance, patience and support for helping me around the laboratory and answering my inquiries. It is through their kind co-operation that I am able to successfully carry out my experiments. Furthermore, I would like to acknowledge my appreciation to CIBA, Cryo-EM and IMRE for allowing me to conduct my experiments in their facilities.

In addition, heartfelt thanks goes to my friends, Jazreel, Yi Herng, Laurentcia, Stacey, Jiayan and Qi Xiang for their continuous support and advices while making the entire journey pleasant and fun.

Special thanks goes to my girlfriend, Yuan Shen, for her endless moral support and understanding, as well as encouragements to help me see the light at the end of the tunnel.

Last but not least, I would like to show my appreciation to my family for showing me love and support throughout my university education.

Contents

List of Figures vii

List of Tables ix

1 Introduction 1

1.1 Electron-beam Writing . . . 2

1.2 Proton-beam Writing . . . 2

1.2.1 Advantages of Protons . . . 2

1.2.2 Drawbacks of Protons . . . 3

2 Aims 4

2.1 Final Aim . . . 4

2.2 Primary Aim . . . 6

2.3 Secondary Aim . . . 6

3 Related Theories 8

3.1 Lithography . . . 8

3.1.1 Types of Photoresist . . . 9

3.2 The Fabrication Techniques . . . 10

3.2.1 Etching . . . 10

3.2.1.1 Reactive-ion Etching(RIE) . . . 11

3.2.1.2 KOH Etching . . . 11

3.2.2 Magnetron Sputtering . . . 13

3.2.2.1 Plasma . . . 13

3.2.3 Focused Ion Beam (FIB) . . . 13

3.3 Ion Source and Brightness 14
3.4 Ion Source Test Bench (ISTB) 15
3.5 Electron Impact Gas Ion Source (Chip) 16
3.6 Aperture 18
3.6.1 Using the Aperture 18

4 Materials & Methods **20**
4.1 Electron Impact Gas Ion Source 20
4.1.1 Fabrication Process 20
4.1.2 Testing Process 26
4.2 Aperture 27
4.2.1 Fabrication Process 34
4.2.2 Assembly Process 37
4.2.3 Measurements 39

5 Results & Discussion **40**
5.1 Electron Impact Gas Ion Source 40
5.1.1 Dimensions Measurements 42
5.1.2 Beam measurement 45
5.2 Aperture 46
5.2.1 Dimensions Measurements 48
5.2.1.1 Difficulties Encountered 51

6 Conclusion **53**

References **55**

A List of Aperture Sizes **56**
A.1 Data Table for Aperture Sizes 56

List of Figures

1.1 Comparison Of Electron Beam And Proton Beam In polymethyl-methacrylate (PMMA) Resist . . . 3

2.1 Overview Of The Final Aim . . . 5
2.2 Proton Beam Writing (PBW) System in CIBA, NUS . . . 7
2.3 1st and 2nd Generation Proton Beam Writers . . . 7

3.1 Comparison of Positive and Negative Photoresists . . . 9
3.2 Selectivity and Isotropy of Etchants . . . 10
3.3 Reactive-ion Etching (RIE) . . . 12
3.4 Potassium Hydroxide (KOH) Etching . . . 12
3.5 Diagram of Ion Source Test Bench (ISTB) . . . 15
3.6 Design of Chip . . . 17
3.7 Gas Chamber Within the Chip. . . . 17
3.8 Design of Aperture . . . 19
3.9 Placement and Usage of Aperture . . . 19

4.1 Fabrication Process for Chip . . . 25
4.2 Testing of Ion Source . . . 26
4.3 Fabrication Process for Aperture . . . 36
4.4 Light Microscope Used for Alignment . . . 38
4.5 Optical Microscope Used for Measurement . . . 39

5.1 Top and Bottom Pieces of Chip Before Gluing . . . 41
5.2 Top View of Chip . . . 41
5.3 Micrograph of Gas Inlet, Top View . . . 42

5.4 Micrograph of Gas Inlet, Bottom View 42
5.5 Micrograph of Electron Inlet 43
5.6 Micrograph of Beam Outlet 43
5.7 Micrograph of Chamber Length and width 44
5.8 Double Aperture Si_3N_4 layers with spacer gap in between 44
5.9 Aperture before cutting 47
5.10 Aperture Top-Bottom Pieces After Cutting 47
5.11 Micrograph of “20μm” Aperture, Initial Opening 48
5.12 Micrograph of “20μm” Aperture, Aperture Size 48
5.13 Micrograph of “10μm” Aperture, Initial Opening 49
5.14 Micrograph of “10μm” Aperture, Aperture Size 49
5.15 Micrograph of “5μm ”Aperture, Initial Opening 50
5.16 Micrograph of “5μm” Aperture, Aperture Size 50
5.17 Problems Encountered During Fabrication 51
5.18 Micrometer Screw Gauge used to measure the thickness of wafer . 52

List of Tables

4.1 Range of Aperture Sizes for 300pA Current (Maximum) 28
4.2 Range of Aperture Sizes for 60pA Current (20% of Max) 29
4.3 Range of Aperture Sizes for 30pA Current (10% of Max) 30
4.4 Range of Aperture Sizes for 15pA Current (5% of Max) 31
4.5 Range of Aperture Sizes for 6pA Current (2% of Max) 32
4.6 Range of Aperture Sizes for 1pA Current (Minimum) 33

5.1 Results from Ion Sources 45

1

Introduction

Mobile phones, laptops, mp3 players, transport systems, are some of the things we used in our day to day life that has some form of integrated circuits in them. These ICs consist of components such as transistors, resistors, insulators, conductors and many more and it might be surprising to many that all those different components are made from the same semiconductor materials through microelectronics processes. As we get more reliant on technologies, we tend to look for more high performance devices while demanding them to be more lightweight and compact. This drives companies into a race to create smaller and better devices. However, for semiconductor devices to be scaled down in size, while integrating moving parts on the chip, it requires more advanced technologies such as smaller micro-electromechanical systems (MEMS) and nano-electromechanical (NEMS) devices.

However, technologies in the current microelectronics production are only capable of two-dimensional (2D) topologies which means that the written pattern will be mainly on the surface [1]. To further reduce the size of the semiconductor devices, we would need high aspect ratio three-dimensional (3D) microstructures with details in the nanometre scale such that the smaller details and deeper depth allows more connections to be made on a smaller area. In order to do that, we need to develop new lithographic techniques suitable to produce high aspect ratio 3D components in both the micro- and nano-scale regime.

1.1 Electron-beam Writing

Current lithography techniques uses electron beam to write the required pattern into the resist. As the electrons from the beam (primary electrons) are light, it would result in a electron-electron interaction which is the deflection of the primary electrons by the electrons in the resist as it permeates the resist thus broadening the beam. This is known as the forward scattering process. However, there are also heavier particles in the resist, such as the substrate nucleus, and the collision of the electrons with these heavy particles is known as the back-scattering process. This also leads to a wider scattering angle of the electrons. Therefore, using electron-beam lithography causes a proximity effects in which the developed pattern will be wider than the scanned pattern [2].

1.2 Proton-beam Writing

To produce high aspect ratio 3D micro- and nano- components, we will need to develop new techniques and this is being done in the Centre for Ion Beam Applications(CIBA). We have developed a proton-beam (P-beam) writing system which uses a focused beam of fast moving protons to write directly into the resist to produce a 3D image in the resist material [3].

1.2.1 Advantages of Protons

Protons are much heavier compared to the electrons. Therefore, due to this mass mismatch ($m_p/m_e \sim 1800$), the primary proton beam tends to generate secondary electrons with much lower energies in the resist as compared to the electron beam due to the conservation of momentum. This results in minimal proximity effect. Furthermore, due to the large mass of the protons, it has significantly less deviations when it encounter collisions as it passes through the resist much like a bowling ball hitting the pins. This enables the proton beam to have the characteristic straight trajectory and high penetration ability, which allow us to produce the high density 3D micro- and nano- structures that we want with smooth side walls.

1.2.2 Drawbacks of Protons

P-beam writing that is being developed in CIBA is currently the only technique that is able to direct-write high aspect ratio 3D nano- and microstructures. As this is a new technology, there is no other instruments available yet and thus we will face difficulties as the p-beam writer is being constructed in CIBA.

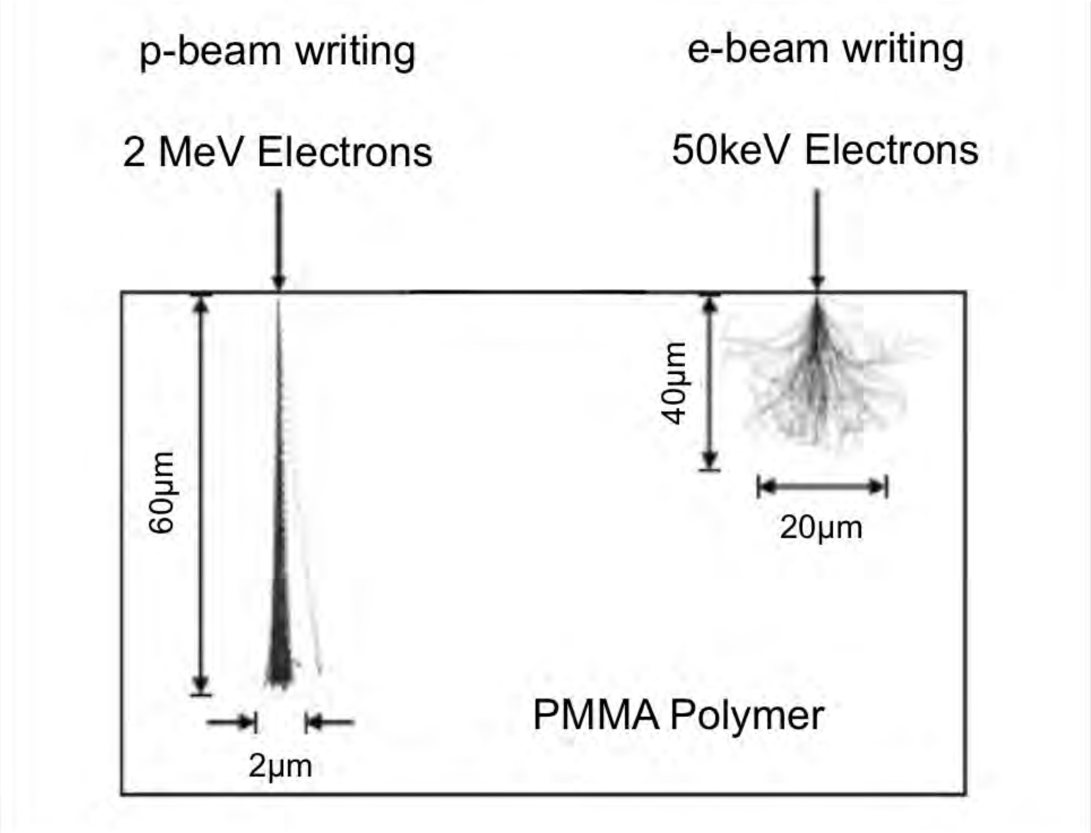

Figure 1.1: Comparison Of Electron Beam And Proton Beam In poly-methylmethacrylate (PMMA) Resist - The left side shows the characteristic straight trajectory and penetration of the proton beam writing with low proximity effect while the right side shows the high proximity effects of using election beam lithography. *Image adapted from pbeam.com.*

2

Aims

2.1 Final Aim

The prototype of the p-beam writer (PBW) that is already available in CIBA is a p-beam writing set-up connected to a 3.5 MV HVEE Singletron™ accelerator [4]. The PBW attached to the accelerator consist of several apertures to narrow the beam size, analyzing magnets that are used to bend the beam in order for the beam to reach the p-beam writing set-up on the beam line and focusing magnets that are also used to focus the beam. The ion source is placed in the accelerator chamber and with high voltage applied, protons are produced and it would have to accelerate through the series of apertures and magnets before it is refocused at the p-beam writing set-up to hit on the target. Due to the long path that the protons have to travel and the constant narrowing of the beam, which allows the bright centre of the beam through, most of the beam intensity are lost and thus the resultant brightness of the beam would be low. Brightness, in this case, is a quantity proportional to the number of particles passing through a unit target area per second.

In the accelerator system, with energy of 2MeV provided to the ion source and an aperture size of 30μm x 30μm, it produces a focused beam with current of 400pA. This gives us a current density of 0.44A/m^2. This shows that the p-beam writer works, however, the estimated brightness of the beam is not as high compared to an existing electron-beam writing system. Thus, the current system

would require a longer period of time just to write on the same length on the resist.

This made it unsuitable for commercial purposes which would require a more efficient system. Therefore, CIBA aims to develop a compact high brightness photon beam writing system that could be used commercially. To achieve this, we would need to find a way to make the whole p-beam writing system (from the accelerator to the PBW set-up) more compact and also to find a way to get an ion beam with higher brightness. This way, once it is done, the new source and the compact accelerating column could be put together with the existing PBW lens set-up to get the more compact high brightness photon beam writing system.

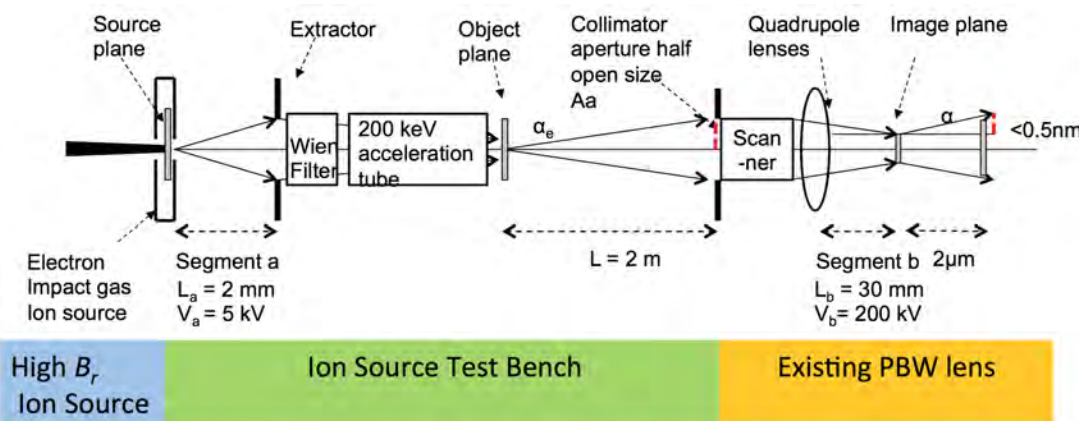

Figure 2.1: Overview Of The Final Aim - From the left, the High brightness ion source would be attached to the compact accelerating column and the existing p-beam writer lens system would be attached to complete the whole proton beam writer.

2.2 Primary Aim

There are two ways to increase the brightness of the proton beam. One of the methods is by reducing the distance that the proton takes to reach the target and the other is to use an ion source that emits high brightness ions. In order to test this while not tempering with the main accelerator's ion source as there are other experiments that uses it, an Ion Source Test Bench (ISTB) was set up. The ISTB was designed and set-up to bring out the full potential of the current radio frequency (RF) source by improving its reduced brightness and it will be also be used to test other high brightness ion source designs in the future. Measurements have been done with the RF source which have an aperture radius of 0.25mm. This gives a beam current measurement of 10nA. Thus giving us a current density of 0.051A/m^2, which is much smaller than the current density of the beam from the accelerator.

To get a high brightness ion source, we would be fabricating and modifying an electron impact gas ion source. This requires the use of several fabrication steps that needs to be adjusted as the project progresses. The whole fabrication phase is a very time-consuming process as we could not proceed to the next step in fabrication process before the previous step is done.

Once the chip is fabricated, we would need another piece of device, an aperture that is capable of measuring the parameters that is needed, to test and measure the brightness of the beam that exit the aperture. This aperture also needs to be designed and fabricated, which is another time-consuming process, more details of the Chip and Aperture will be discussed in Chapter 3.

2.3 Secondary Aim

After the Chip and Aperture are fabricated, the secondary aim is to fit them into the ISTB and have it tested on making holes in graphene layer so that this could be used as a filter for water molecules.

Regrettably, we were unable to achieve our secondary and final goal due to the limited time constraint.

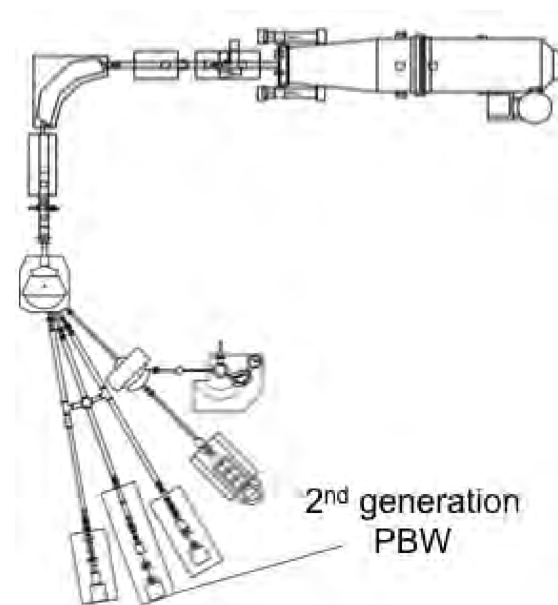

Figure 2.2: Proton Beam Writing (PBW) System in CIBA, NUS - The Main Singletron™ accelerator in Center for Ion Beam Applications (CIBA), Physics, NUS, is connected to 5 beam lines and the 2nd Generation PBW is located at the 20° beam line.

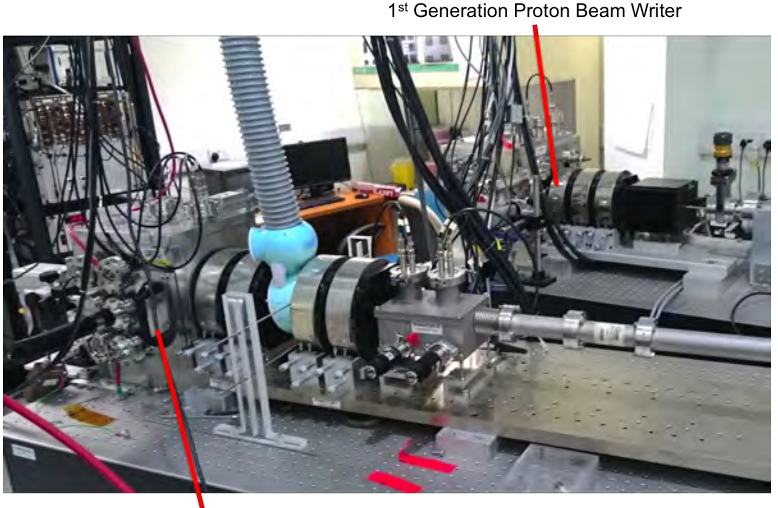

Figure 2.3: 1st and 2nd Generation Proton Beam Writers - The PBW at the back of the image is the 1st generation while the one nearer is the 2nd generation PBW system.

3

Related Theories

In this chapter, I'll go through some of the relevant terms and theories for better understanding of this project.

3.1 Lithography

Writing a desired pattern on a piece of substrate (eg, silicon wafer) or on a layer of thin film starts with the process known as lithography. Of the many known methods of lithography, the first method is to make a mask of the desired pattern, which is very much made like a piece of paper with a shape cut out from it. When the mask is placed under the light source, usually ultra-violet (UV) light, the light will only pass through the pattern. This is how light is used to transfer the pattern to a light-sensitive "photoresist" which would be layered on top of the substrate. This method is known as photolithography [5].

Another method is electron beam (e-beam) lithography , where instead of using light and a mask, a focused beam of electrons directly writes the pattern on the resist [6]. The purpose of the two mentioned methods is to create very small structures. However, the downside of using electrons is due to the high proximity effects as structures made using e-beam lithography are two-dimensional. Thus, we tend to improve this by using protons instead and create a p-beam writing system.

There are also other lithography techniques that are available, such as X-ray lithography and interference lithography, but they will not be discussed here.

3.1.1 Types of Photoresist

To use lithography, a layer of the light-sensitive resist is needed on the substrate. There are 2 types of photoresists, positive photoresist and negative photoresist. For positive photoresist, the chemical structure of the resist changes when light shines on it, making it soluble in the developer. This will leave the unexposed section after developing, in other words, “whatever shows goes” thus leaving an exact copy of the pattern on the wafer.

The negative resist is just the opposite. Instead of becoming soluble when exposed to light, the exposed area would polymerise, making it difficult to be washed off by the developer solution. This then only allows the developer to remove the unexposed area, leaving only the exposed area. Therefore, mask used with the negative photoresist have the inverse of the desired pattern [7].

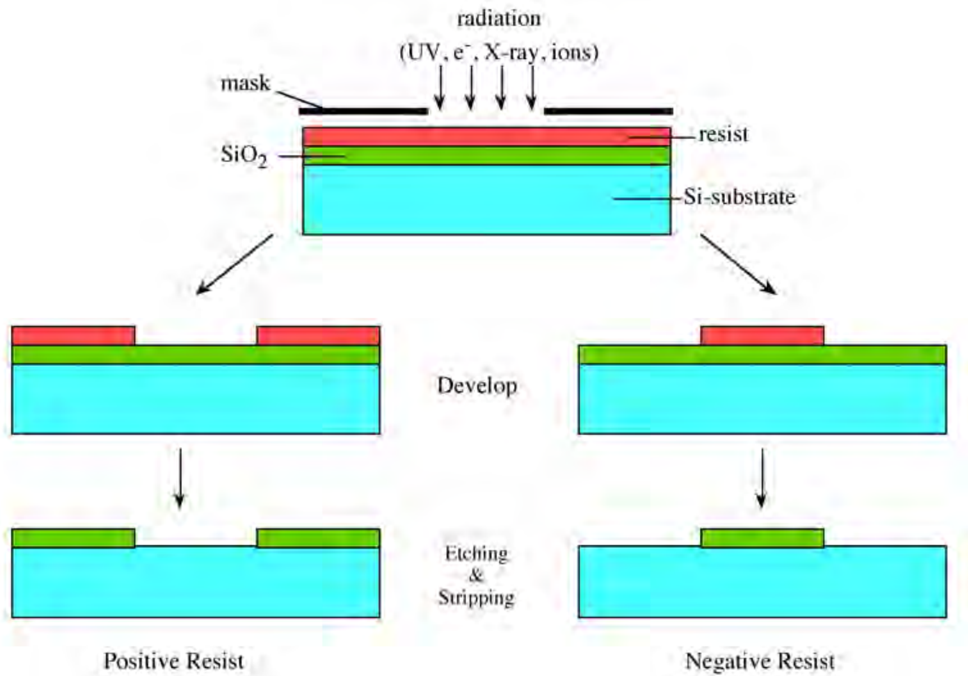

Figure 3.1: Comparison of Positive and Negative Photoresists - The left side shows the outcome of using a positive photoresist where it leaves an exact copy of the pattern after developing while the right hand side shows the inverse pattern when a negative photoresist is used. *Image adapted from cnx.org.*

3.2 The Fabrication Techniques

3.2.1 Etching

Once the desired pattern is "engraved" into the resist, transferring the patten onto the wafer uses a technique known as etching, which remove layers of the substrate from the surface of the wafer. The photoresist used should be resistant to etching and thus protects the unexposed part of the wafer from the etchants used.

The amount of substrate to be etched is then controlled approximately by noting the amount of etching time spent, the etching rate and the selectivity of the etchant used. Some etching processes would create an undercut beneath the resist causing sloping sidewalls (isotropic) while some would produce vertical sidewalls (anisotropic). Thus, depending on what is needed, wafers usually went through many etching processes before completion with there being many different ways to etch. However, I will only be looking at 2 etching processes, mainly reactive-ion etching (RIE) and potassium hydroxide (KOH) etching.

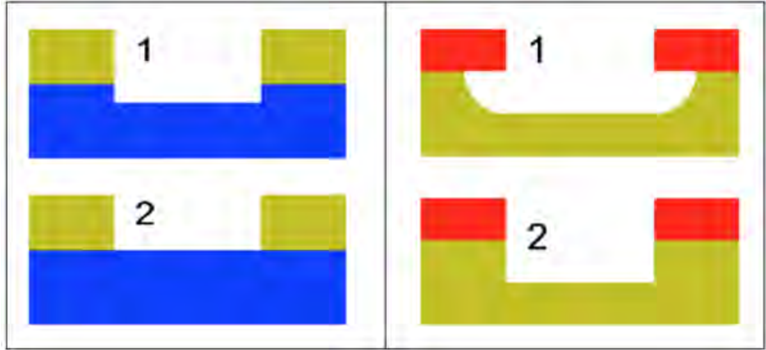

Figure 3.2: Selectivity and Isotropy of Etchants - (On the left) The blue layer shown is the layer to remain. **1** shows a poorly selective etch in which the material underneath has been etched while **2** shows a highly selective etch which leaves the material underneath untouched. **(On the right)** The red layer is the resist and the yellow is the layer to be removed. **1** shows a isotropic etch which erodes the substrate in all directions creating round sidewalls while **2** shows a anisotropic etch with vertical sidewalls. *Image adapted from wikipedia.*

3.2.1.1 Reactive-ion Etching(RIE)

RIE is a dry etching process which uses a chemically reactive plasma to remove materials that are on the wafer. Plasma is generated in the chamber by applying an oscillating radio frequency (RF) electromagnetic field which removes the electrons from the gas molecules [8]. The free electrons will then be accelerated both downwards towards the wafer and upwards to the top of the chamber. The electrons that hit the chamber walls would be absorbed and conducted to the ground while the rest is deposited onto the wafer platter thereby charging it up.

Due to the large voltage difference between the slight positive charge of the plasma (due to the positive ions) and the huge negatively charged wafer platter, it would cause the positive ions to be attracted to the wafer platter. Upon colliding with the sample, a chemical reaction would occur between the sample's surface material and the ions causing the surface substrate to be used up, thus removing layers of the substrate. In addition, the ions could also transfer its kinetic energy to the material, knocking it off the surface (sputter).

3.2.1.2 KOH Etching

The second method uses "wet" etchants which requires the wafer to be submerged in the etchant and different wet etchants would etch the different exposed face of a crystal at different rates (anisotropic etching). For the etching of silicon, KOH is used. Its etch rate in the $\langle 100 \rangle$ crystal direction is 400 times higher than in the $\langle 111 \rangle$ direction. Therefore, when etching $\langle 100 \rangle$ silicon through a square hole, it will create a slope sidewall of $\langle 111 \rangle$ silicon with a flat $\langle 100 \rangle$ bottom where the flat bottom will disappear if the etching is allowed to "complete" [9]. The $\langle 111 \rangle$-oriented sidewall and the surface of the wafer creates an angle of:

$$\theta = \arctan \sqrt{2} = 54.7^\circ \tag{3.1}$$

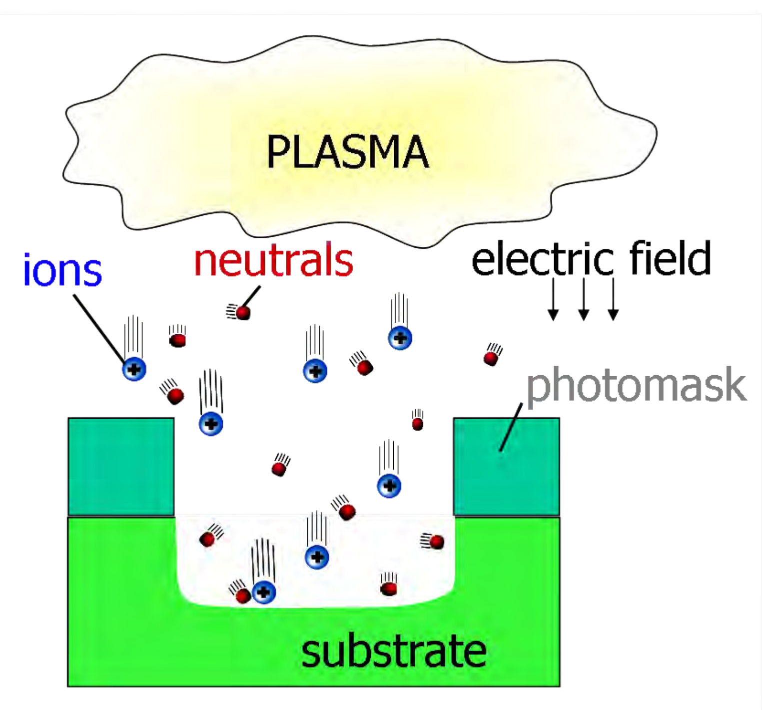

Figure 3.3: Reactive-ion Etching (RIE) - Schematic diagram of RIE showing the direction of the electric field and the flow of the ions from the plasma towards the substrate in response to the electric field. *Image adapted from scorec.rpi.edu.*

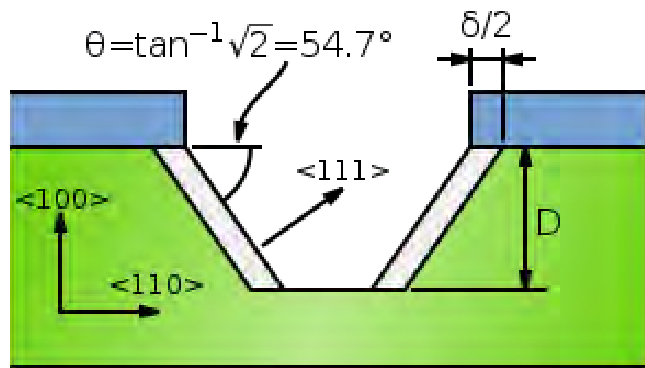

Figure 3.4: Potassium Hydroxide (KOH) Etching - Cross section of an etched silicon wafer with sloping sides of $\langle 111 \rangle$ planes and the bottom of flat $\langle 100 \rangle$ plane. The top blue layer is the resist, and the green area is silicon substrate. *Image adapted from wikipedia.*

3.2.2 Magnetron Sputtering

Some of the wafers needs to have conductive layers so as to draw away accumulated charge, to act as a connector, etc and this can be done by a sputtering process. In basic sputtering process, the target, which is the deposition material, is the cathode while the substrate (wafer) is the anode. Ions generated in the plasma, which is located in front of the target, would accelerate towards the target. The bombardment of ions on the target allows energy to be transferred from the ions to the target atoms, thus breaking the bonds holding the atoms. The "sputtered" atoms would flow towards the substrate and condense as a thin film. Furthermore, the ions bombardment on the target surface would also cause secondary electrons to be emitted. These ions are used to maintain the plasma.

However, the basic process has low deposition rates and low efficiencies in the ionization in the plasma. Therefore, current sputtering uses a magnetic field that is parallel to the target surface to constrain the secondary electrons near the target to overcome the limitations. This is known as Magnetron Sputtering [10].

3.2.2.1 Plasma

Plasma is a gas cloud full of positive and negatively charged particles and usually inert gas, such as argon, would be used to generate the plasma. A potential difference would be applied between the cathode and anode to create an electric field. This electric field caused electrons to flow from the cathode to the anode. Due to the gas molecules in between, the electrons would collide with these molecules causing excitation, dissociation and ionization of the gas molecules and this coexistence of the ions with the free electrons is plasma.

3.2.3 Focused Ion Beam (FIB)

FIB system is similar to the scanning electron microscope (SEM) except that it uses a focused beam of ions instead of electrons. Using these ions, FIB can have several uses, the first is to use FIB is for imaging purposes, and the second is to use it as a machining tool due to its sputtering capability, we will be using the latter.

3.3 Ion Source and Brightness

An ion source is a device that forms molecular and atomic ions after a large amount of energy is applied to a gas. However, there are many ways that the ions in the source could be created such as through electron ionization, chemical ionization, plasma source, etc. The RF source used in the ISTB uses plasma created from radio frequency voltage to generate the ions. This RF source can be operated with any type of gas (e.g. Hydrogen, Oxygen, Argon. etc.) and it can be used for experiments that requires the constant usage of the source.

The electron impact gas ion source that we are building and modifying uses electron ionization which uses "energetic electrons" to interact with the gas atoms or molecules to produce the ions. These "energetic electrons" will be from an electron gun situated in a Scanning Electron Microscope (SEM). The beam of electrons will be directed to the entrance of the reservoir of gas for ionization.

The property that is needed from an ion source for the proton beam writing system is for it to produce a high quality proton beam. Quality of a charged particle beam is usually determined by the beam size and the current density, with smaller beam size and high current density being the most desirable. However, reduced brightness, B_r, would be used to determine the quality of the beam instead of current density as current density, $J = I/A$, is included in the calculation of reduced brightness and that B_r also includes the energy spread of the beam.

The reduced brightness of a point source is given by:

$$B_r = \frac{I}{A_s(\frac{A_0}{D^2})V} \tag{3.2}$$

where B_r is the reduced brightness with units of A/m^{2}SrV, I is the current, A_s is the area of the aperture at the source, A_0 is the area of the aperture near the substrate, D is the distance between the two apertures and V is the potential difference applied [11].

3.4 Ion Source Test Bench (ISTB)

The ISTB is currently attached with an RF source. The RF source is filled with the gas which we are interested in and with a supply of RF voltage (∼100MHz), it will produce plasma. The ions filled plasma would then be extracted using a extraction voltage between 0 to -3kV through a 2mm canal. The beam would then be accelerated as it passes through a series of metal electrodes (acceleration column), which acts as potential dividers across the high voltage to the ground terminal. The accelerated beam passes through a Wein filter assembly after it was collimated with a nickel aperture (0.5mm). The Wein filter is used to select the mass and charge of the ions that would be allowed to pass through undeflected through another nickel collimator (0.5mm) before hitting the target [12].

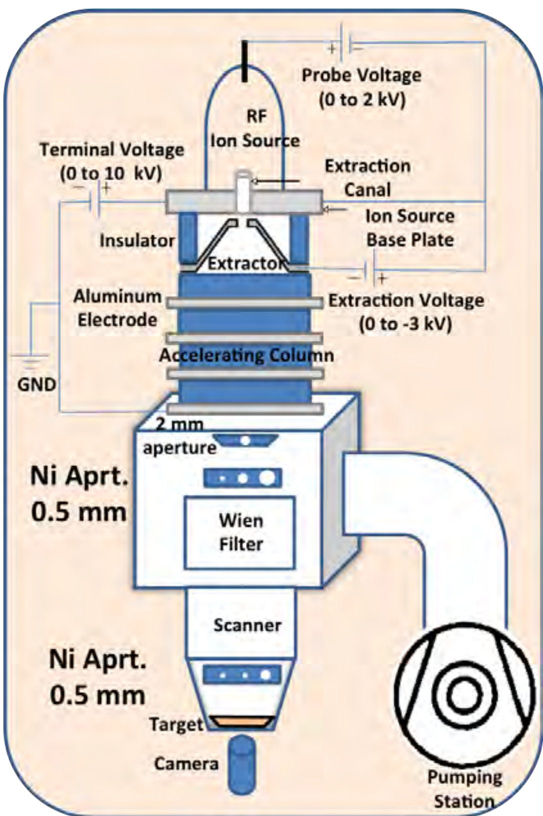

Figure 3.5: Diagram of Ion Source Test Bench (ISTB) - Diagram shows the set up of the ISTB with the accelerating column, Wein filter, sizes of the nickel apertures and the respective voltages across it.

3.5 Electron Impact Gas Ion Source (Chip)

It could be seen from equation above that a small aperture would increase the reduced brightness of the beam. Thus, we proceed to find an ion source with an aperture as small as possible. Based on the designs by Charged Particle Optics group in Delft University of Technology, we decided to develop a modified version of an electron impact gas ion source [13]. The concept behind the chip is to direct an electron beam into the gas chamber through a small double aperture between 100nm to 1μm in diameter. The gas chamber would be located between the two apertures. The ions produced by electron impact inside the gas chamber are being extracted by an electric field applied across the double aperture. There would also be an extractor plate placed after the chip. The chip would be fabricated using two 530 μm thick $\langle 100 \rangle$ Si wafer with 1μm thick of Si_3N_4 on both sides.

By using Si wafer to make an ion source, the space between the 2 wafer used would determine the distance of the parallel plate (double apertures) at which an electric field would be to prevent the free electrons from emitting from the source as we only require the ions. As the equation for the electric field is given by: $E = \frac{V}{d}$ where E is the electric field, V is the potential difference and d is the distance between the parallel plate.

It can be seen that with a small separation d, a small potential difference applied would result in a large electric field. This would also beneficial as a lower potential difference applied would mean that V in equation above would be small and it would then further increase the reduced brightness of the beam. Therefore, a small bias voltage (1V - 9V) is used to generate the electric field and depending on the position that the gas gets ionised, the ions will end up having a range of initial energy with 9eV for ions ionising at the top and 1eV for ions at the most bottom [12].

As seen from the figure below, gas would be fed into the chip through the bigger inlet on the left and fill the chamber in the middle. Electrons from an electron gun will ionized the gas from the top inlet on the right hand side. Using an ion extractor placed after the chip, the protons will be extracted from the exit at the bottom of the chip.

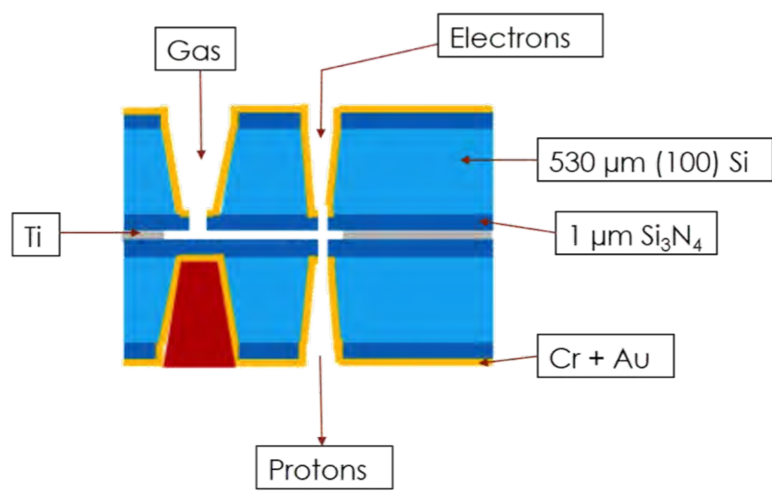

Figure 3.6: Design of Chip - Cross section of the ion source using 530μm thick ⟨100⟩ Si wafer with 1μm thick of Si_3N_4 on both sides and labels of the inlet for the gas and electron beam and outlet for the ions. The chromium (Cr) and gold (Au) layer is used to apply the potential difference.

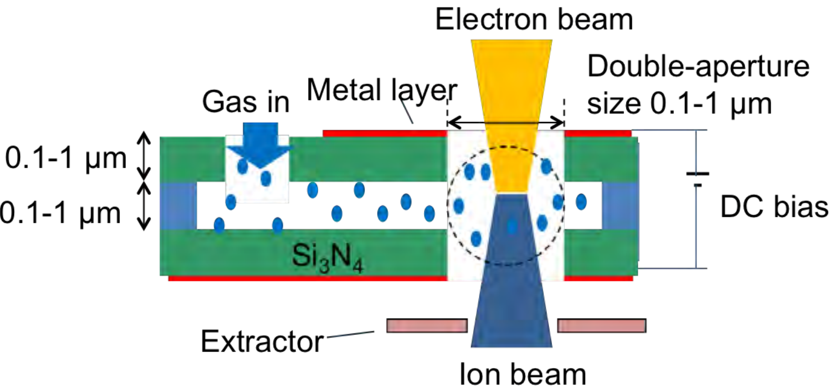

Figure 3.7: Gas Chamber Within the Chip. - The opening on the left is the gas inlet. The gas will be confined in the chamber where it will be ionized by the electron beam through the double aperture on the left. The conversion efficiency of ionizing the gas from the electron beam is given by the ratio of the current density of ions to electrons and it is equals to the product of the ionization cross section (m^2), length of electron's path (m) and the gas particle density (m^{-3}) [14]. This gives us a efficiency of 0.055% for protons and 1.3% for Ar^+. The extractor is used to prevent excess electrons from passing through and accelerating the ions. *Image taken from [12].*

3.6 Aperture

To measure the brightness of the ion beam once the chip is done, we would need a tool to measure all the parameters needed to calculate the brightness of the beam. The beam brightness that I am interested in is for the beam after it passes through the aperture. Currently, current from the beam that is emitted directly from the chip have been measured using a Faraday cup, and with the size of the exit aperture known, we could calculate the current density. However, to find the brightness of the beam, we would need to know the solid angle which is given by $\Omega = A_0/D^2$ [15].

In order to know what aperture sizes are required to measure the reduced brightness, some assumptions and estimations have to be made. These estimations were based on the measurements we get when we tested the chip (more details in chapter 4). I then calculated a range of aperture sizes that could be used and devised a fabrication process for these apertures to be made.

3.6.1 Using the Aperture

The "Aperture" that I am fabricating would also consist of a small double aperture. The bottom layer would be connected to ground through a conductive layer of sputtered Cr and Au so that excess charge as the beam passes through the aperture would not accumulate in the aperture and affect the beam. The aperture would have different range of opening sizes, thus if the opening size is smaller then the beam size, the aperture would limit the beam size passing through the aperture. This would reduce the beam current passing through and it would be the current used to measure the reduced brightness. Knowing the exit window of the aperture and the distance separating the double aperture, the solid angle could be calculated and this is another quantity that is needed. From this, we would have the values for the beam current I, solid angle Ω, potential difference V and source aperture size A_s to calculate the reduced brightness B_r of the ion beam. Similar to the chip, the aperture uses a 525μm thick $\langle 100 \rangle$ Si wafer with 200nm Si_3N_4 layers on both sides.

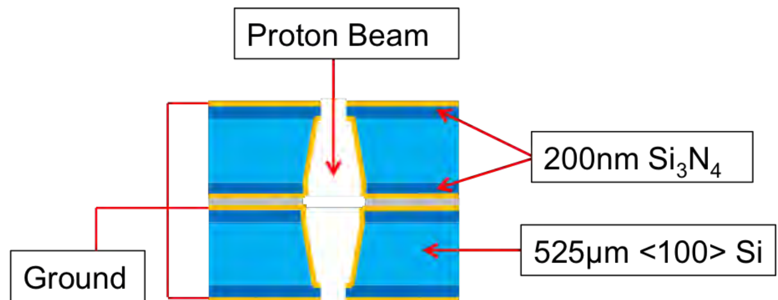

Figure 3.8: Design of Aperture - Cross section of the aperture using 525μm thick ⟨100⟩ Si wafer with 200nm thick of Si_3N_4 on both sides. Conductive layer, sputtered from Cr and Au, is used to remove excess charge.

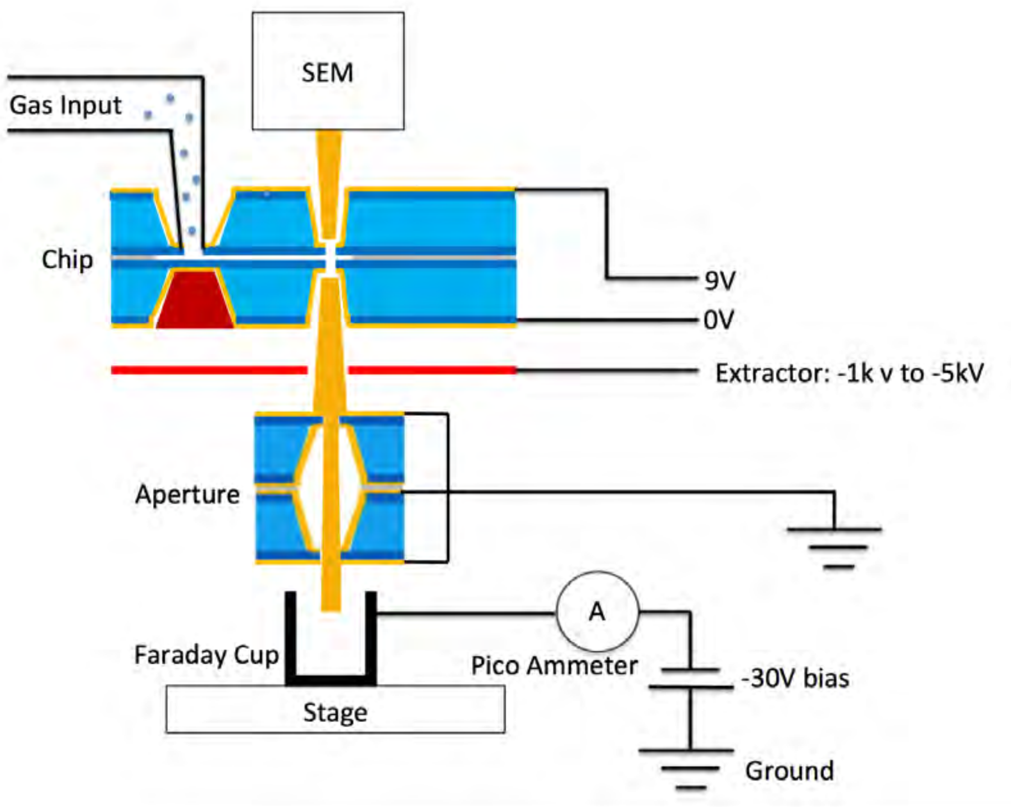

Figure 3.9: Placement and Usage of Aperture - The aperture is place below the extractor plate to focus and narrow the emitted ion beam as well as to aid in the calculation of the reduced brightness.

4

Materials & Methods

4.1 Electron Impact Gas Ion Source

4.1.1 Fabrication Process

The fabrication process of the chip and apertures involves several key steps and it was done together with my colleagues, Liu Nannan and Xu Xinxin. The main feature for the chip would be the miniature gas chamber. The chip is fabricated by firstly spin coating a layer of positive photoresist, AZ 1518, onto one side of the Si wafer. The pattern design for the gas and electron beam inlets is then loaded into the laser writer to write into the resist, and AZ1518 developer is used to remove the exposed area.

RIE etching is then used to etch the Si_3N4 layer while KOH etching, which is most commonly used for silicon etching at the micro level, is used to etched the silicon layer. This would leave a layer of free-standing Si_3N4 to form the 300μm x 300μm and 50μm x 50μm windows on the top of the chip. Sputtering is done to deposit a thin conductive layer of Cr and Au metal ($\sim$ 20nm) on the chips surface for the application of a bias voltage across the chip.

As the top and bottom of the chip are similar, except for the gas window at the bottom which is not needed, we decided to use the same piece for both, thus simplifying the fabrication process. However, additional fabrication steps is needed to be applied to the bottom pieces of the chip to create the gas chamber.

The gas chamber which is of dimensions 6mm(L) x 1mm(W) x 200nm(H) in between the top and bottom wafers first started off with a layer of positive photoresist, AR-P 3250, applied on the Si_3N4. Ultra-violet (UV) light is used instead of the laser writer to transfer the pattern onto the resist as the pattern for the chamber does not require the fine beam of the laser. 200nm of Cr and Ti (Titanium) is deposited after to be used as the spacer before the excess resist is removed. Once the top and bottom pieces are done, the 2 parts are aligned and glued together before using FIB milling to penetrate the last layer of Si_3N4. The opening for the gas inlet and double aperture are 20μm x 20μm and 1.5μm respectively [12].

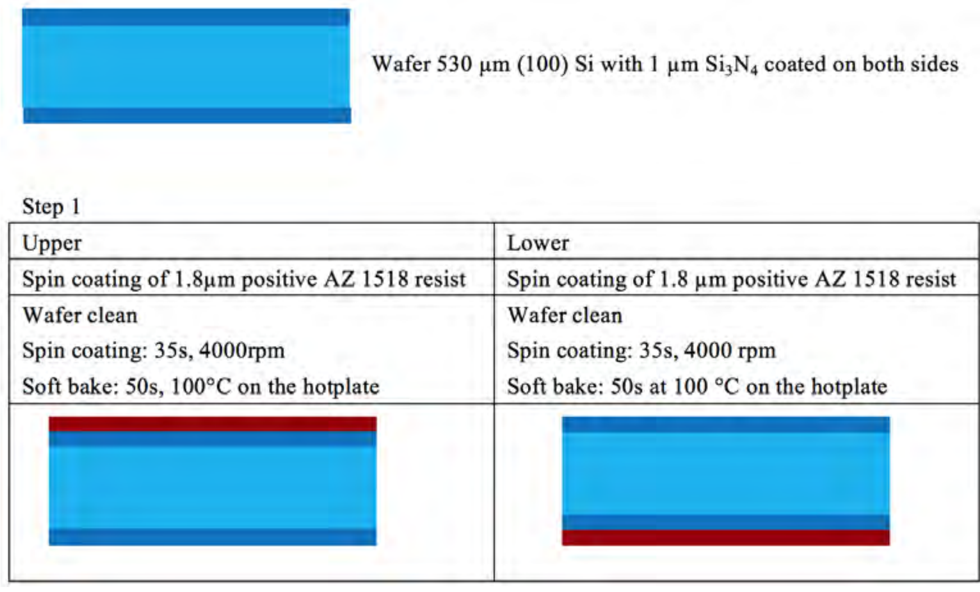

Step 1

Upper	Lower
Spin coating of 1.8µm positive AZ 1518 resist	Spin coating of 1.8 µm positive AZ 1518 resist
Wafer clean Spin coating: 35s, 4000rpm Soft bake: 50s, 100°C on the hotplate	Wafer clean Spin coating: 35s, 4000 rpm Soft bake: 50s at 100 °C on the hotplate

Step 2

Upper	Lower
Exposing of pattern	Exposing of pattern
Exposure: laser writer at 405nm, 25mW, 100% Develop: AZ 400k developer: DI water = 1:4, 1 minutes	Exposure: laser writer at 405nm, 25mW, 100% Develop: AZ 400k developer: DI water = 1:4, 1 minutes

Step 3

Upper	Lower
RIE etching	RIE etching
Use 55 sccm CHF_3 and 5 sccm O_2 at 175 W RF power and 55 mTorr for 50 minutes	Use 55 sccm CHF_3 and 5 sccm O_2 at 175 W RF power and 55 mTorr for 50 minutes

Step 4

Upper	Lower
KOH etching	KOH etching
Remove AZ 1518 resist using acetone Use 20% KOH at 85 °C. Water bath for 4.5 ~ 5 hours	Remove AZ 1518 resist using acetone Use 20% KOH at 85 °C. Water bath for 4.5 ~ 5 hours

Step 5

Upper	Lower
Magnetron sputtering for conductive layer	Magnetron sputtering for conductive layer
Deposit Cr layer for 15s to give about 10 nm Deposit Au layer for 20s to give about 14 nm	Deposit Cr layer for 15s to give about 10 nm Deposit Au layer for 20s to give about 14 nm

Step 6

Write mask
Using laser writer at 405 nm, 15 mW, 100% Develop with AZ 400k developer: DI water = 1:4 for 1 minute (~ 500 nm AZ1518) Chrome etching for 2 minutes (~ 500nm Cr)

Step 7

Upper	Lower
	Spin coating 3.5 µm positive AR-P 3250 resist
	Clean Wafer Spin coating: 60 s at 8000 rpm for 3.5 µm Soft bake: 2 minutes at 95 °C on the hotplate, then a slow cooling to avoid stress cracks

Step 8

Upper	Lower
	Exposure pattern
	Exposure: Using UV at 365 nm and 100 W power supply for 3.5 minutes (recommended value is 220 mJ/cm^2) Develop with AR 300-26 developer: DI water = 3:2 for 1.5-2 minutes

Step 9

Upper	Lower
	Magnetron sputtering
	Deposit Cr layer for 15s to give about 10 nm Cr Deposit Ti layer for 20 minutes to give about 290 nm Ti

Step 10

Upper	Lower
	Remove resist
	Use acetone to remove resist, let it sit for about 30 minutes

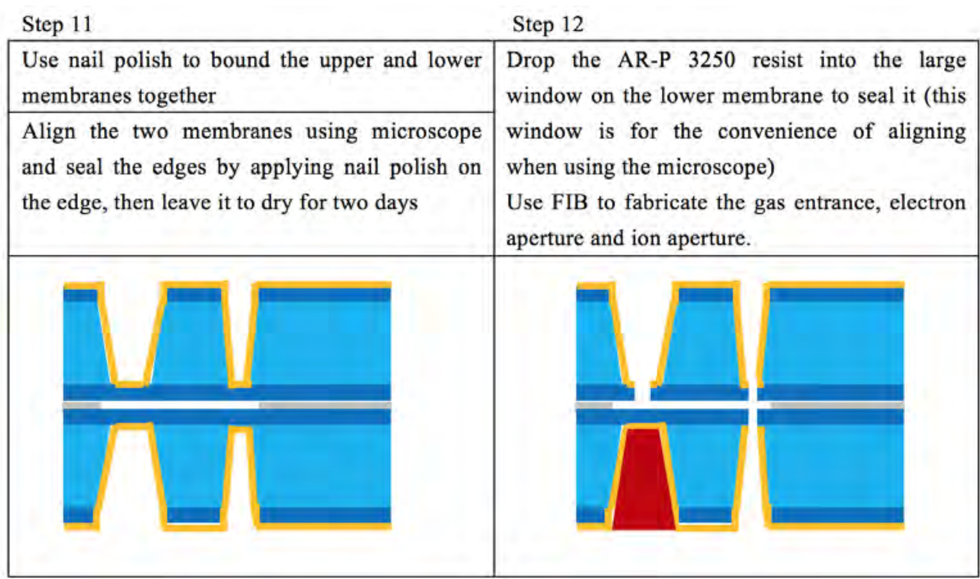

Step 11	Step 12
Use nail polish to bound the upper and lower membranes together	Drop the AR-P 3250 resist into the large window on the lower membrane to seal it (this window is for the convenience of aligning when using the microscope)
Align the two membranes using microscope and seal the edges by applying nail polish on the edge, then leave it to dry for two days	Use FIB to fabricate the gas entrance, electron aperture and ion aperture.

Figure 4.1: Fabrication Process for Chip

4.1.2 Testing Process

Testing the chip requires an electron source to ionise the gas in the chamber and this was achieved by using the electron gun in a scanning electron microscope (SEM) system (Philip XL30) located in NUS. A gas regulating valve is also used to vary the gas inlet pressure from 1mbar to 2bar. A bias voltage of up to 9V is applied to generate the electric field mentioned. The extractor plate is placed 1.5mm below the chip with an extraction voltage between −1keV and −5keV and it has an opening size of 1mm.

Once the system is set-up, an electron beam of 1keV beam energy is injected into the double aperture from the top to ionize the gas. The ion beam produced is measured using a Faraday cup placed 1.5mm below the extractor plate with a bias of −30V. The extraction plate's voltage will always be set to a much higher negative value so as to prevent the incident electrons from passing through and reaching the Faraday cup. It also prevents secondary electron emitted from the Faraday Cup from leaving.

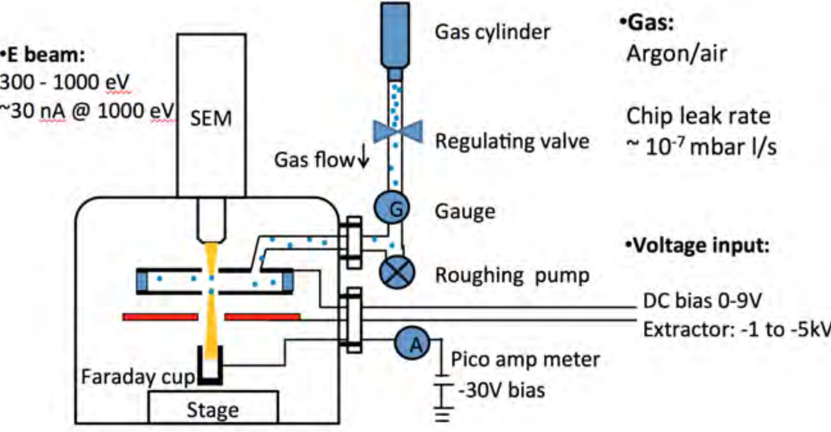

Figure 4.2: Testing of Ion Source - Schematic set-up of ion source in the SEM in NUS showing the positions of each items in details of how the testing is done. It also shows the voltage input for the chip, extractor and Faraday cup and also the energy input of the electron beam. *Image taken from [13].*

4.2 Aperture

The window sizes for the aperture will determine how much of the beam will be allowed through and this will determine the beam current and thus the brightness. The double aperture and the distance between them will also determine the solid angle. Thus, calculating the sizes of the apertures to be used is important for the achievement of high brightness beam. To calculate the aperture sizes, we would need to have the values for the reduced brightness as well as the the window area that is nearest to the target, A_o. However these are specifically the values that I am supposed to get from the aperture itself. Thus, the aperture sizes were back-calculated using estimations for the beam current, I and the reduced brightness of the beam that would pass through the aperture.

Assumption that the aperture windows at the top and bottom of the "Aperture" are the same were made as this would firstly make the fabrication process easier and secondly, this would assume that the incoming beam are parallel. Estimation of the beam current through the aperture is done by looking at the beam current that is being measured from the electron gas impact ion source and the RF source from the ISTB. The current measured from the chip would be the maximum current, and it is known that when the current passes through the aperture it will be significantly reduced. However, the amount of current being reduced is not known. Therefore, to get the suitable range of window sizes, I will include a range of possible values for the beam current ranging from 1pA (smallest) to 30pA (10% of the maximum). Same goes for the value for the reduced brightness. Brightness measurements taken from the RF source from the ISTB with ion current of 300pA, diameter of 0.5mm for each aperture, 0.45m for the distance between the 2 apertures, and an energy of 1keV for the He^+ ions, gives a reduced brightness of 1.6 A/m^2(rad)eV. Since I want a high brightness beam, I estimated the values of the brightness up to 1000A/m^2(rad)eV. Using these values, it can be seen from the tables below that the safe range of apertures is from 3μm to 15μm for brightness level of lowest 20 A/m^2(rad)eV. Thus, aperture size of 5μm, 10μm and 20μm is to be made. The larger 20μm is made so as to ensure that the beam could pass through the larger window first before shifting the aperture to a smaller window.

Ion Beam Current (pA)	**Energy** (eV)	**Brightness** (A/m^2(rad)eV)	**Aperture** (μm)
300	1200	1.58	22.52
300	1200	25.00	11.28
300	1200	50.00	9.49
300	1200	100.00	7.98
300	1200	400.00	5.64
300	1200	800.00	4.74
300	1200	1000.00	4.49
300	100	1.58	41.91
300	100	2.50	21.00
300	100	5.00	17.66
300	100	100.00	14.85
300	100	400.00	10.50
300	100	800.00	8.83
300	100	1000.00	8.35

Table 4.1: Range of Aperture sizes for 300pA current (Maximum) - Keeping the current at 300pA, the maximum and minimum value for the energy input was chosen to find out the 2 extreme aperture sizes. Brightness ranges from that of the ISTB to as high as 1000A/m^2(rad)eV.

Ion Beam Current (pA)	**Energy** (eV)	**Brightness** (A/m^2(rad)eV)	**Aperture** (μm)
60	1200	1.58	15.06
60	1200	20.00	7.98
60	1200	40.00	6.71
60	1200	100.00	5.34
60	1200	200.00	4.49
60	1200	400.00	3.77
60	1200	600.00	3.41
60	1200	800.00	3.17
60	1200	1000.00	3.00
60	100	1.58	28.01
60	100	20.00	14.85
60	100	40.00	12.49
60	100	100.00	9.93
60	100	200.00	8.35
60	100	400.00	7.02
60	100	600.00	6.35
60	100	800.00	5.91
60	100	1000.00	5.58

Table 4.2: Range of Aperture sizes for 60pA current (20% of Max) - Keeping the current at 20% of maximum value, the maximum and minimum value for the energy input was chosen to find out the 2 extreme aperture sizes. Brightness ranges from 1.58 to as high as 1000A/m^2(rad)eV.

Ion Beam Current (pA)	**Energy** (eV)	**Brightness** (A/m^2(rad)eV)	**Aperture** (μm)
30	1200	1.58	12.66
30	1200	20.00	6.71
30	1200	40.00	5.64
30	1200	100.00	4.49
30	1200	200.00	3.77
30	1200	400.00	3.17
30	1200	600.00	2.87
30	1200	800.00	2.67
30	1200	1000.00	2.52
30	100	1.58	23.55
30	100	20.00	12.49
30	100	40.00	10.50
30	100	100.00	8.35
30	100	200.00	7.02
30	100	400.00	5.91
30	100	600.00	5.34
30	100	800.00	4.97
30	100	1000.00	4.70

Table 4.3: Range of Aperture sizes for 30pA current (10% of Max) - Keeping the current at 10% of maximum value, the maximum and minimum value for the energy input was chosen to find out the 2 extreme aperture sizes. Brightness ranges from 1.58 to as high as 1000A/m^2(rad)eV.

Ion Beam Current (pA)	**Energy** (eV)	**Brightness** (A/m^2(rad)eV)	**Aperture** (μm)
15	1200	1.58	10.65
15	1200	20.00	5.64
15	1200	40.00	4.74
15	1200	100.00	3.77
15	1200	200.00	3.17
15	1200	400.00	2.67
15	1200	600.00	2.41
15	1200	800.00	2.24
15	1200	1000.00	2.12
15	100	1.58	19.81
15	100	20.00	10.50
15	100	40.00	8.83
15	100	100.00	7.02
15	100	200.00	5.91
15	100	400.00	4.97
15	100	600.00	4.49
15	100	800.00	4.18
15	100	1000.00	3.95

Table 4.4: Range of Aperture sizes for 15pA current (5% of Max) - Keeping the current at 5% of maximum value, the maximum and minimum value for the energy input was chosen to find out the 2 extreme aperture sizes. Brightness ranges from 1.58 to as high as 1000A/m^2(rad)eV.

Ion Beam Current (pA)	**Energy** (eV)	**Brightness** (A/m^2(rad)eV)	**Aperture** (μm)
6	1200	1.58	8.47
6	1200	20.00	4.49
6	1200	40.00	3.77
6	1200	100.00	3.00
6	1200	200.00	2.52
6	1200	400.00	2.12
6	1200	600.00	1.92
6	1200	800.00	1.78
6	1200	1000.00	1.69
6	100	1.58	15.76
6	100	20.00	8.35
6	100	40.00	7.02
6	100	100.00	5.58
6	100	200.00	4.70
6	100	400.00	3.95
6	100	600.00	3.57
6	100	800.00	3.32
6	100	1000.00	3.14

Table 4.5: Range of Aperture sizes for 6pA current (2% of Max) - Keeping the current at 2% of maximum value, the maximum and minimum value for the energy input was chosen to find out the 2 extreme aperture sizes. Brightness ranges from 1.58 to as high as 1000A/m^2(rad)eV.

Ion Beam Current (pA)	**Energy** (eV)	**Brightness** (A/m^2(rad)eV)	**Aperture** (μm)
1	1200	1.58	12.66
1	1200	20.00	6.71
1	1200	40.00	5.64
1	1200	100.00	4.49
1	1200	200.00	3.77
1	1200	400.00	3.17
1	1200	600.00	2.87
1	1200	800.00	2.67
1	1200	1000.00	2.52
1	100	1.58	23.55
1	100	20.00	12.49
1	100	40.00	10.50
1	100	100.00	8.35
1	100	200.00	7.02
1	100	400.00	5.91
1	100	600.00	5.34
1	100	800.00	4.97
1	100	1000.00	4.70

Table 4.6: Range of Aperture sizes for 1pA current (Minimum) - Keeping the current at 1pA, the maximum and minimum value for the energy input was chosen to find out the 2 extreme aperture sizes. Brightness ranges from 1.58 to as high as 1000A/m^2(rad)eV.

4.2.1 Fabrication Process

The fabrication process is shorter for the aperture due to its simpler design. Firstly, similar to the chip, AZ 1518 is spin coated onto the wafer, and the laser writer is used to write the pattern. AZ 1518 developer is used to develop the resist. RIE etching and KOH etching is used to etch the Si_3N4 and Si layers respectively. Finally, Cr and Au are sputtered on as a conductor to ground the aperture so as to remove the excess charge accumulated in the aperture. For the aperture, the top and bottom pieces are identical therefore fabrication can be done together. The top and bottom are aligned and glued together before the double aperture through the Si_3N4 layers are removed using FIB milling.

As the aperture would be placed in a vacuum environment, addition precaution needs to be taken when assembling the top and bottom pieces. To prevent breakage of the aperture due to the pressure difference, an opening is needed to allow the air to escape while the vacuum is created. This is done when piecing the 2 parts together, small strips of double-sided tapes are placed on 2 sides to secure the top and bottom pieces, while air are allowed to leave from the 2 opened sides.

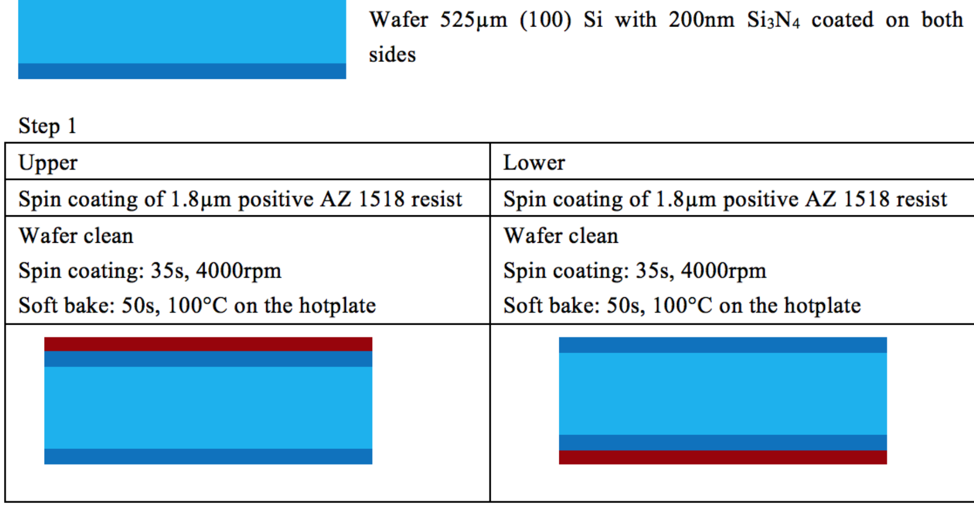

Step 1

Upper	Lower
Spin coating of 1.8µm positive AZ 1518 resist	Spin coating of 1.8µm positive AZ 1518 resist
Wafer clean Spin coating: 35s, 4000rpm Soft bake: 50s, 100°C on the hotplate	Wafer clean Spin coating: 35s, 4000rpm Soft bake: 50s, 100°C on the hotplate

Step 2

Upper	Lower
Exposing of pattern	Exposing of pattern
Exposure: laser writer at 405nm, 25mW, 100% Develop: AZ 400k developer: DI water = 1:4, 1 minutes	Exposure: laser writer at 405nm, 25mW, 100% Develop: AZ 400k developer: DI water = 1:4, 1 minutes

Step 3

Upper	Lower
RIE etching	RIE etching
Use 55 sccm CHF_3 and 5 sccm O_2 at 175 W RF power and 55 mTorr for 15 minutes	Use 55 sccm CHF_3 and 5 sccm O_2 at 175 W RF power and 55 mTorr for 15 minutes

Step 4

Upper	Lower
KOH etching	KOH etching
Remove AZ 1518 resist using acetone Use 20% KOH at 85 °C. Water bath for 4.5 ~ 5 hours	Remove AZ 1518 resist using acetone Use 20% KOH at 85 °C. Water bath for 4.5 ~ 5 hours

Step 5

Upper	Lower
Magnetron sputtering for conductive layer on both sides	Magnetron sputtering for conductive layer on both sides
Deposit Cr layer for 15s to give about 10 nm Deposit Au layer for 20s to give about 14 nm	Deposit Cr layer for 15s to give about 10 nm Deposit Au layer for 20s to give about 14 nm

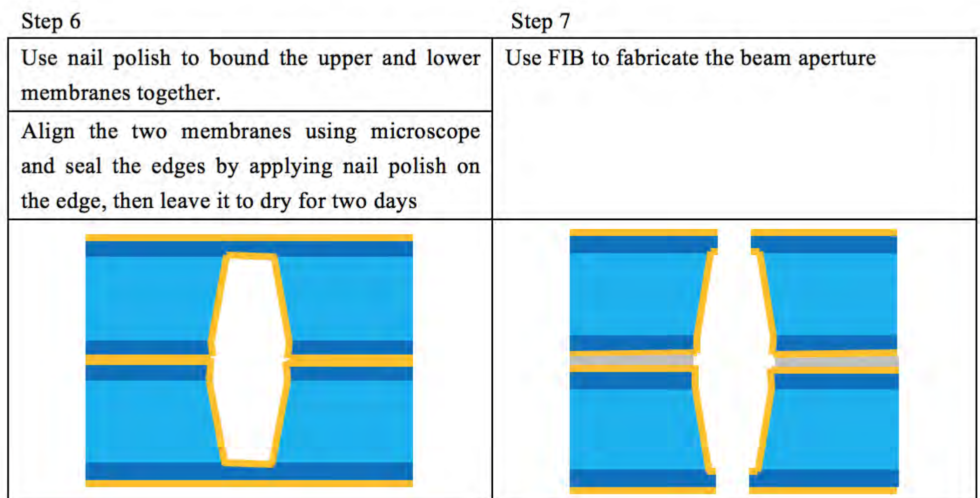

Step 6	Step 7
Use nail polish to bound the upper and lower membranes together.	Use FIB to fabricate the beam aperture
Align the two membranes using microscope and seal the edges by applying nail polish on the edge, then leave it to dry for two days	

Figure 4.3: Fabrication Process for Aperture

4.2.2 Assembly Process

Once the top and bottom "apertures" were fabricated, they need to be broken into their individual pieces. This is done by firstly aligning the lines of the pattern on the wafer to the length edge of a glass slide. Pressure is added to the parts on the glass slide to keep it in place while a small amount of pressure is applied to the edge that is hanging off the glass slide to fracture the silicon along the etched line. This would result in strips of wafers. The same method is done again to break them into individual pieces.

The individual top and bottom pieces would need to be glued together. This is done by having the top and bottom windows aligned together using a light telescope with the aid of a moving stage with 3 micrometer screw gauge for each axis. The apertures are adhered onto glass slides with the help of tiny droplets of water. The slide with the top aperture is clamped onto the movable stage while the slide with the bottom aperture is placed on a separate stationary stage. The stage is then adjusted in the x- and y-direction so that the window of the top piece overlaps the bottom piece. Once aligned, the top piece is lowered onto the bottom piece using the z-direction micrometer screw gauge.

The 2 glass slides is held firmly while binder clips were used to secure them together. A small amount of nail polish is applied to the perimeter of the half exposed top-bottom assembly using a sharpened wooden skewer since the other half is inaccessible due to the glass slides. The assembly is then left to dry for a day before the top glass slide could be removed. Nail polish is then applied to the remaining half and left to dry for another day. Once fully dried, the aperture is gently scraped off the glass slide using a razor blade and the excess nail polish are trimmed off before it is kept in a dry box to await further testing.

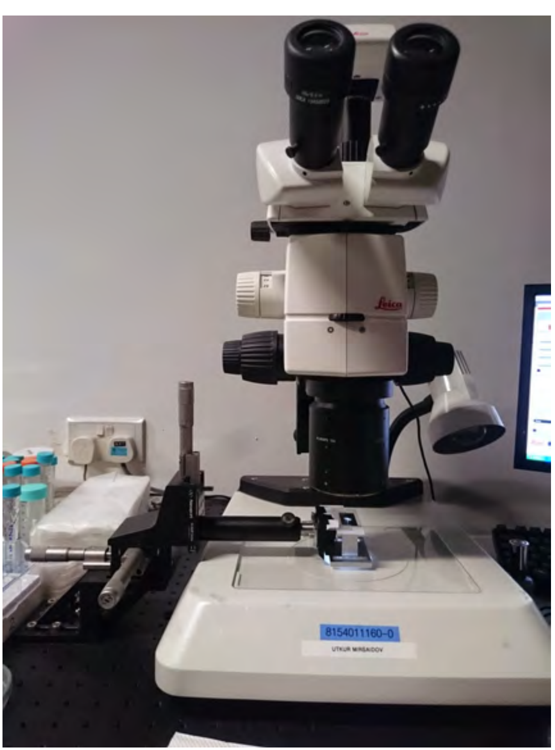

Figure 4.4: Light Microscope Used for Alignment - The top piece of the double aperture sticks onto a glass slide with aid of tiny droplets of water and secured to a 3-axis movable stage. The bottom piece also sticks to the glass slide with water but it is placed on a stationary stage. Using the microscope to look through the window, the top piece is slowly maneuvered in the x- and y-direction over the bottom piece till the double aperture aligns before it is lowered and glued.

4.2.3 Measurements

After the assembly of the aperture is done, measurements of the fabricated aperture are taken using an optical microscope to ensure that the aperture chip have been made according to the theoretical values. This is due to that the fabrication process is not fixed and that the process would vary slightly depending on the amount of chemical used or the energy used for the laser writer when writing the pattern.

Moreover, since we are fabricating our own chips and apertures, we would need to do a first trial of fabrication to know the limitations of our machinery and through this trial and error, we could know what is needed to improve to get a more accurate chip in the future.

Since the chip was already being fabricated by Nannan and Xinxin, the trial and error process is mainly done for the aperture that I am fabricating since this will be the first batch of aperture chips to be fabricated.

Figure 4.5: Optical Microscope Used for Measurement - Varying magnifying lens could be switched to view at higher magnifications.

5

Results & Discussion

In this chapter, I will be presenting the fabricated chips and apertures as well as comparing the measured dimensions of these chips to their theoretical intended value. Each prototype chip and aperture are first inspected using an optical microscope with varying magnifications and measurement taken. Measurements, stated in this chapter, are all done on the top and bottom pieces of the chips separately (before gluing) and the units stated below each micrograph shows the units of the values in the micrograph.

5.1 Electron Impact Gas Ion Source

As a quick reminder, the chips produced are being developed as a modified electron gas ion source and there will be various windows for the gas of interest, the electron beam entrance and ion beam exit as shown in Figure 3.6. All the windows are connected to a reservoir where the gas is stored for the electron beam to collide for the production of ions and that reservoir can be seen from the black rectangular strip below. The chip with yellowish colored layer (bottom of image) on the surface where the reservoir is on is the spacer. Cr and Au was initially used to create the spacer thus explaining the yellowish-gold color. However, since we do not require the conductive gold layer and due to high cost, we decided to replace it with Ti instead. The other side of the chip (top right) is coated with Cr and Au as a conductive layer is needed to apply a potential difference. However, since it is a very thin layer ($\sim$ 20nm), it does not have the distinct gold color.

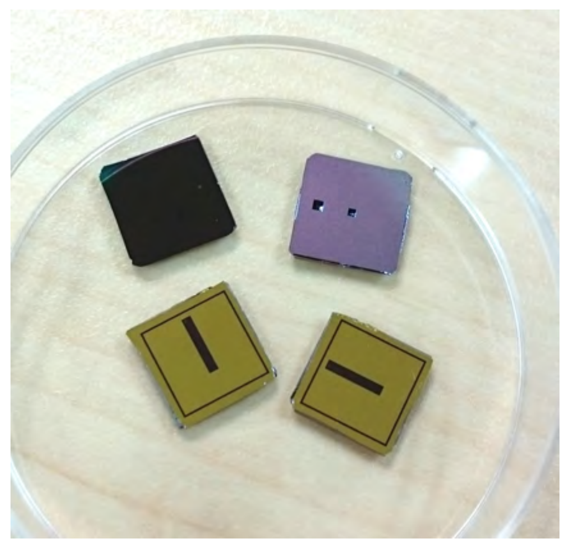

Figure 5.1: Top and Bottom Pieces of Chip Before Gluing - The yellowish pieces at the bottom shows the bottom half of the Ion Source with the gas chamber being the black rectangular shape in the middle. The top right piece is the top half of the chip.

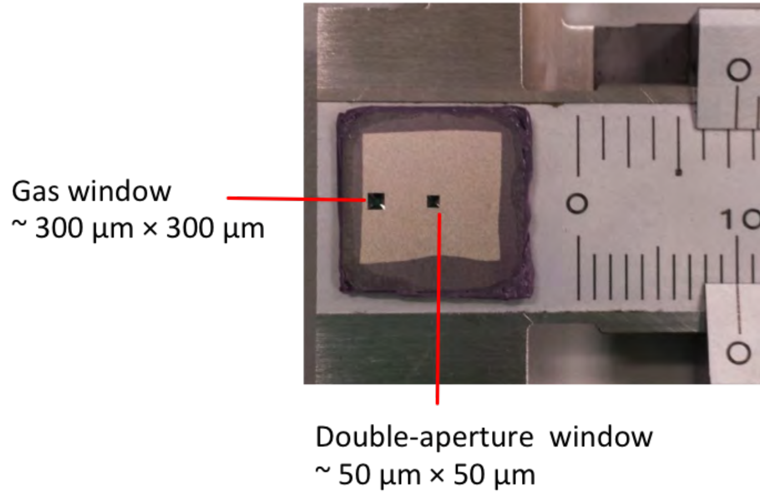

Figure 5.2: Top View of Chip - The left hole is the gas inlet opening while the right is the double aperture for the electron beam.

5.1.1 Dimensions Measurements

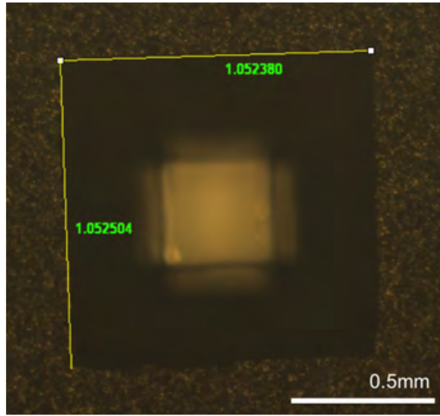

Figure 5.3: Micrograph of Gas Inlet, Top View

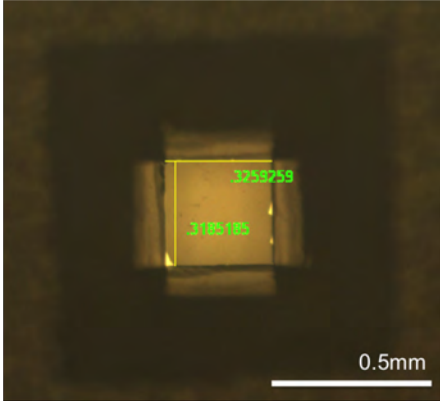

Figure 5.4: Micrograph of Gas Inlet, Bottom View

With reference to Figure 3.6, the gas window is the top left most opening. Theoretically, for the gas inlet to achieve the small opening of 0.300mm x 0.300mm, an initial opening of 1.049mm x 1.049mm is needed before KOH etching. This was achieved in the chips that was made where the initial opening size was measured to be 1.052mm x 1.053mm which gives the final smaller opening of 0.319mm x 0.326mm.

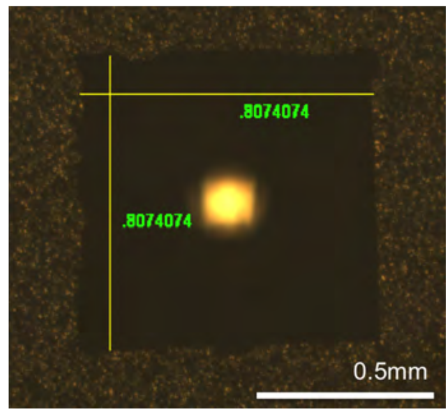

Figure 5.5: Micrograph of Electron Inlet

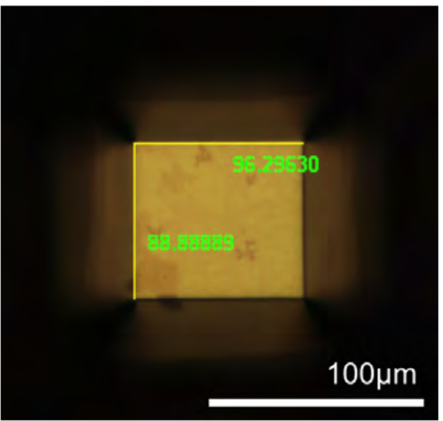

Figure 5.6: Micrograph of Beam Outlet

Similarly, for the double aperture on the right of Figure 3.6, 0.799mm x 0.799mm initial opening was to be made to give a 50.0μm x 50.0μm opening for the narrow window in the center. However, after fabrication, although an initial opening of 0.807mm x 0.807mm, which is very close to the theoretical value, was made, the smaller window was measured to be 96.2μm x 88.9μm. This further shows that the fabrication process varies slightly during fabrication and that we could not get the value that we want exactly.

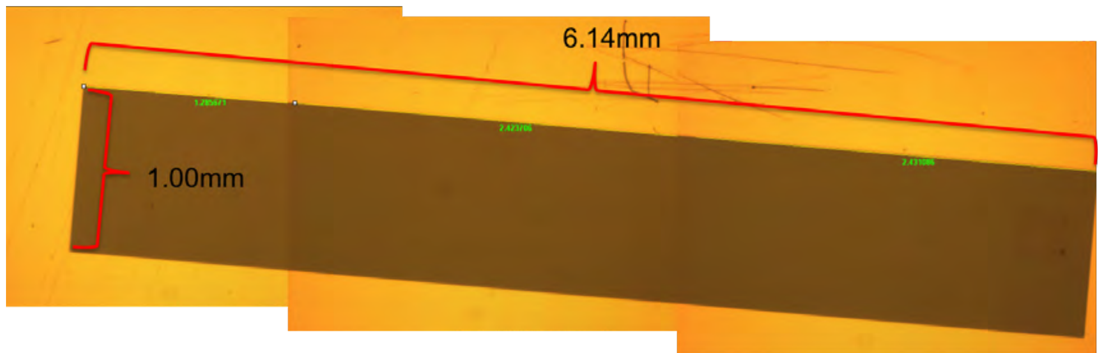

Figure 5.7: Micrograph of Chamber Length and width

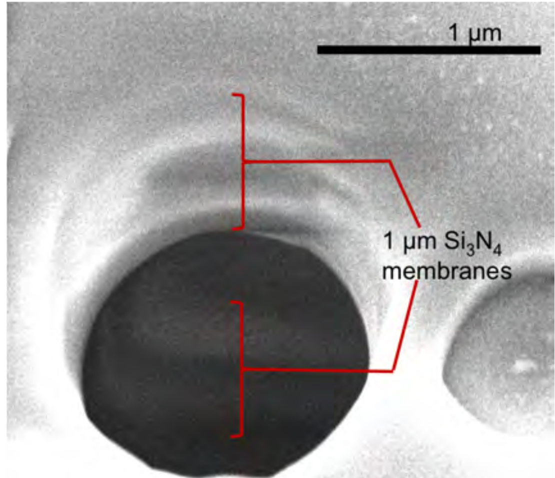

Figure 5.8: Double Aperture Si_3N_4 layers with spacer gap in between

The dimensions of the reservoir was measured to be 6.14mm x 1.00mm with the height being the spacer height which is 200nm. These measurements falls within the intended values of 6mm x 1mm x 200nm.

The measurements of the chip fabricated seems to conform well to the theoretical value thus it would seemed that the fabrication process is accurate. However, as this was started by Nannan and Xinxin, they could have done multiple trails before to know the fabrication parameters to get accurate structures.

5.1.2 Beam measurement

Measurements of the beam from the different sources were done so as to allow us to estimate the Chip's performance as well as to give us a expected value when the actual measurements are to be made.

	Chip	**ISTB(RF Source)**	**Accelerator**
Current	300pA	300pA	400pA
Aperture Size	1.5μm	0.25mm	30μm x 30μm
Energy	30eV	1keV	2MeV
Current Density	$42.4\frac{A}{m^2}$	$0.0015\frac{A}{m^2}$	$0.44\frac{A}{m^2}$

Table 5.1: Results from Ion Sources - Table showing the current density of the different ion sources

Although the brightness measurements could not be made for the Electron Impact Gas Ion Source, Chip, we could still measure the current of the beam coming out of the source and also the aperture sizes of the outlet of each source. This allows us to calculate the current density of the ion beam. Using this value, we could temporarily compare the beam as current density is proportional to the beam reduced brightness. As seen from the table, the current density of the beam from the chip is approximately 100 times more than that of the beam from the 2nd generation prototype PBW thus this would also mean that the brightness of the chip could be 100 times brighter.

My colleagues have already further calculated the brightness of the beam from the ISTB which gives us a value of 1.58A/m^2(rad)eV. Looking at the current density value and the equation for reduced brightness, the current density of the chip is of the order of 10^4 times higher than from the beam of the ISTB, and with the size of the aperture from the chip being smaller and using a smaller energy, it could be seen that the reduced brightness of the beam from the chip could potentially be much higher than the RF source.

However, the reduced brightness of the beam from the chip can only be measured once the aperture is fabricated.

5.2 Aperture

From the calculations done in chapter 4, the range of apertures needed, to be able to test for ion beams with energy between 100eV to 1200eV and current between 1pA to 60pA, are between 1.08μm to 14.85μm. Thus, I recommend apertures of sizes 5μm, 10μm and 20μm. The 20μm aperture was recommended so as to allow experimenters to easily target the ion beam to the center of the aperture before shifting to the smaller apertures. Similarly to the chip above, the measurements of the aperture dimensions are done before the assembly process.

As this is the first batch of apertures to be produced, I do not want to fabricate using a full wafer, thus the design for the apertures were done on a quarter piece wafer with approximately 7 pieces of each aperture sizes as shown in Figure 5.9. Since the small difference between the aperture sizes could not be seen with the naked eye, I added a "marker", denoted as an arrowhead, before each set to help identify the set.

Fabrication of the wafer was time consuming as mentioned as the wafer used was a 525μm thick silicon wafer with a thinner 200nm later of Si_3N4 which was different from the wafer used for the chip, thus the parameters such as the laser writer's beam energy and the etching time needs to be recalculated. This is in addition to the time take for each step processes.

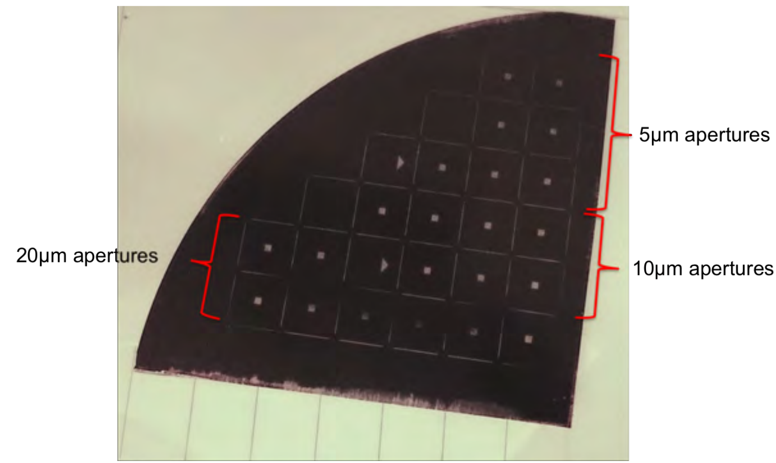

Figure 5.9: Aperture before cutting

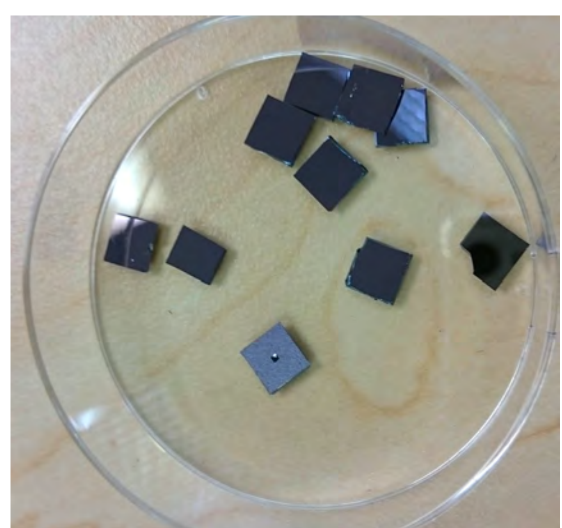

Figure 5.10: Aperture Top-Bottom Pieces After Cutting

5.2.1 Dimensions Measurements

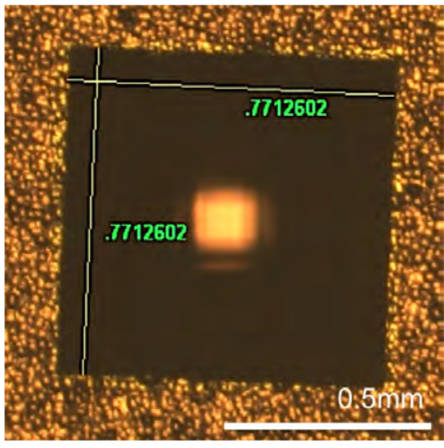

Figure 5.11: Micrograph of "20μm" Aperture, Initial Opening

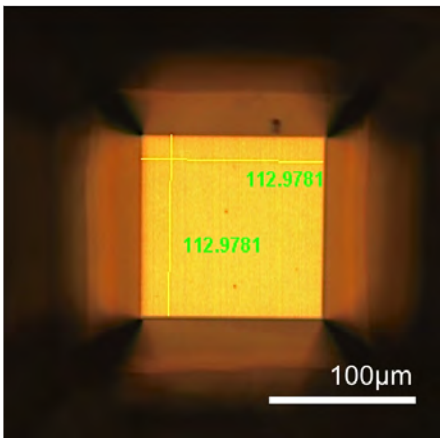

Figure 5.12: Micrograph of "20μm" Aperture, Aperture Size

As KOH etching etched silicon at an angle of 54.7°, there will be a larger initial opening and a smaller window (aperture) after etching. Therefore, for the 9.0μm Aperture, the larger opening window was to be 0.762mm x 0.762mm however, it was 0.09mm bigger (0.771mm x 0.771mm) when it was measured. This would mean that the aperture size would be 0.009mm bigger, which is 29.0μm. But when the aperture size was measured, it was 112.9μm x 112.9μm.

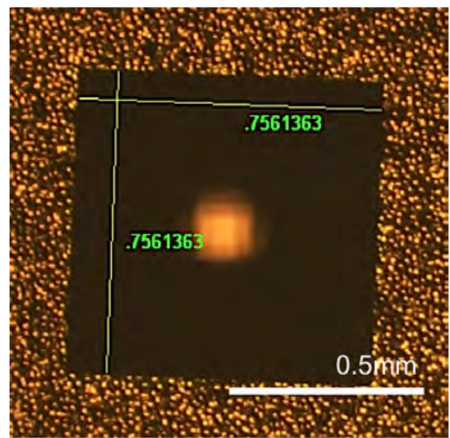

Figure 5.13: Micrograph of "10μm" Aperture, Initial Opening

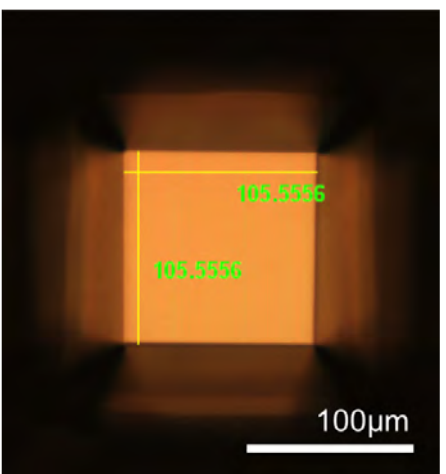

Figure 5.14: Micrograph of "10μm" Aperture, Aperture Size

For the 10μm aperture, an initial opening of 0.752mm x 0.752mm was required to achieve the 10.0μm x 10.0μm aperture theoretically. However, an initial opening of 0.756mm x 0.756mm was measured under the optical microscope which was 0.007mm larger which would theoretically make the aperture size 4μm larger too ($\sim$17μm). However, the measure aperture size was 105.6μm x 105.6μm which is several times larger than expected.

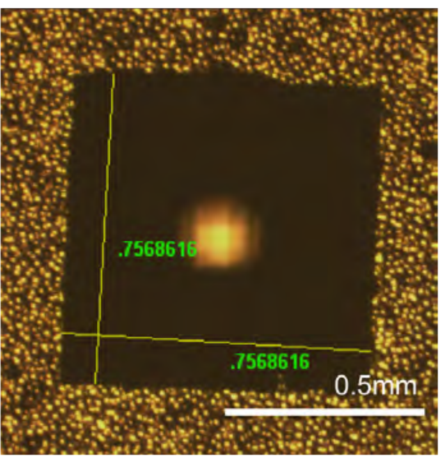

Figure 5.15: Micrograph of "5μm "Aperture, Initial Opening

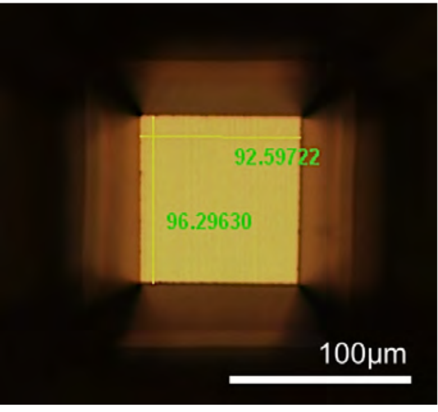

Figure 5.16: Micrograph of "5μm" Aperture, Aperture Size

Same analysis could be done with the final 5μm aperture, initial opening size of 0.757mm x 0.757mm was measured which is 0.010mm larger than the intended 0.747mm x 0.747mm. This would change the expected aperture size to 10μm. However the measured aperture size was 92.6μm x 96.3μm which is also larger than the expected.

5.2.1.1 Difficulties Encountered

Fabrication

There are a few problems that I encountered when I was fabricating the aperture. The first was the alignment of the design to the center of the quartered wafer. The design have to be aligned to the center of the wafer so that there would not be any parts of the designed out of the wafer area. If the design was off the wafer, I would need to remove the resist layer and spin-coat on the resist again before writing. The photoresist needs to be kept put of while light before writing.

After writing, the next problem was the development of the resist, initially when developing the resist, the resist developer was contaminated, thus when the resist was placed in the developer for the required time, it did not develop as expected and if it was left for too long, the resist not written by the laser writer was removed too. Thus, I had to rewrite the pattern and developed it with a new developer. This 2 steps are the most important steps as the following steps after was done systematically.

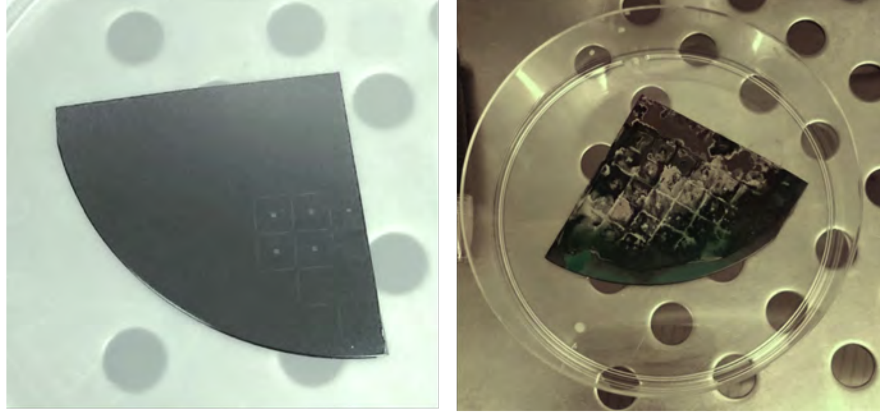

Figure 5.17: Problems Encountered During Fabrication - (**Left**) Misaligned pattern after laser writing. (**Right**) Wafer after being left in the developer longer than expected.

Measurements

As seen above, all the aperture sizes were larger than expected. These larger size could be due to several reasons. Firstly, it could be the wafer thickness was not 525μm thus this would cause the aperture to be bigger as calculations were done based on the given thickness of the wafer. Therefore measurements were done using a digital micrometer screw gauge, the thickness of the wafer was found to be 492μm instead. Thus, based on the measurements of the initial opening of the aperture and using equation 3.1, it was calculated that the aperture sizes are to be 75.2μm, 60.2μm and 61.2μm for the "20μm", "10μm" and "5μm" aperture respective. This would explains the larger aperture sizes.

The second reason could be that the concentration of KOH to deionized(DI) water was not concentrated enough thus the wafer was left in the KOH solution for a much longer period of time, this could cause the KOH to etch into the $\langle 111 \rangle$ direction which would cause the aperture to increase in size slightly. This adds to the explanation of the larger measured aperture sizes as compared to the theoretical aperture sizes calculated based on the 492μm wafer thickness.

The third reason could be that the initial opening window got enlarged a little, during the RIE process to etch the Si_3N_4 layer, as the ions used for RIE could remove the resist layer at the edge of the written pattern. This slight enlargement of the initial opening would cause the aperture window to be larger.

Figure 5.18: Micrometer Screw Gauge used to measure the thickness of wafer

6

Conclusion

We have developed an ion source consisting of a gas chamber with 2 windows of 300μm x 300μm and 50μ x 50μ for the gas inlet and double aperture (where ionization occurs) respectively. We have examined the dimensions of the ion source fabricated and also test the functions of the ion source using a SEM as the electron source. The results show that the dimensions of the chip after fabrications were all within the theoretical dimensions needed and it also gives a beam current density of 42.4A/m^2.

Reduced brightness of the focused beam could be calculated once the aperture sizes are known. The range of apertures were back-calculated from an estimated range of brightness values as well as the beam energy and sizes 5μm, 10μm and 20μm were suggested. The apertures were prototyped and features of the apertures were found to be much larger than the intended values where the supposed 5μm, 10μm and 20μm aperture window sizes have a measured value of 92.6μm, 105.5μm and 112.9μm respectively. The larger aperture window was found that it could be due a thinner wafer of 492μm instead. As calculations was done using 525μm, a smaller thickness would result in larger aperture sizes.

The apertures will still be used for testing while plans for a new batch of apertures are made, and finally we will proceed with the measurement of the ion beam's reduced brightness. We plan to assemble the entire proton beam writing system using the accelerating column from the ISTB, the ion source fabricated and the current lens system available and hopefully revolutionize the nano-fabrication industries.

References

[1] Saul Griffith, Mark Mondol, David S. Kong, and Joseph M. Jacobson. **Nanostructure fabrication by direct electron-beam writing of nanoparticles**. *Journal of Vacuum Science & Technology B: Microelectronics and Nanometer Structures*, **20**(6):2768, December 2002. 1

[2] T. H. P. Chang. **Proximity effect in electron-beam lithography**. *Journal of Vacuum Science and Technology*, **12**(6):1271, November 1975. 2

[3] Jeroen a. Van Kan, Andrew a. Bettiol, Kambiz Ansari, Ee Jin Teo, Tze Chien Sum, and Frank Watt. **Proton beam writing: a progress review**. *International Journal of Nanotechnology*, **1**(4):464, 2004. 2

[4] J. a. Van Kan, P. G. Shao, K. Ansari, a. a. Bettiol, T. Osipowicz, and F. Watt. **Proton beam writing: A tool for high-aspect ratio mask production**. *Microsystem Technologies*, **13**:431–434, 2007. 4

[5] M.D. Levenson, N.S. Viswanathan, and R.A. Simpson. **Improving resolution in photolithography with a phase-shifting mask**. *IEEE Transactions on Electron Devices*, **29**(12):1828–1836, December 1982. 8

[6] R. F. W. Pease. **Electron beam lithography**. *Contemporary Physics*, **22**(3):265–290, September 2006. 8

[7] School of Electrical Georgia Tech and Computer Engineering. **Positive and Negative Photoresist**, 2015. 9

[8] Gottlieb S. Oehrlein. **Reactive-Ion Etching**. *Physics Today*, **39**(10):26, January 1986. 11

[9] a Introduction and B Wafer Cleaning. **Wet-Chemical Etching and Cleaning of Silicon**. *High Temperature*, **22401**(January):0–02, 2003. 11

[10] P.J Kelly and R.D Arnell. **Magnetron sputtering: a review of recent developments and applications**. *Vacuum*, **56**(3):159–172, March 2000. 13

[11] Roland Szymanski and David N. Jamieson. **Ion source brightness and nuclear microprobe applications**. *Nuclear Instruments and Methods in Physics Research Section B: Beam Interactions with Materials and Atoms*, **130**(1-4):80–85, 1997. 14

[12] Nannan Liu, P. Santhana Raman, Xinxin Xu, Huei Ming Tan, Anjam Khursheed, and Jeroen a. van Kan. **Development of ion sources: Towards high brightness for proton beam writing applications**. *Nuclear Instruments and Methods in Physics Research Section B: Beam Interactions with Materials and Atoms*, pages 1–6, 2015. 15, 16, 17, 21

[13] D.S. Jun, V.G. Kutchoukov, C.T.H. Heerkens, and P. Kruit. **Design and fabrication of a miniaturized gas ionization chamber for production of high quality ion beams**. *Microelectronic Engineering*, **97**:134–137, September 2012. 16, 26

[14] Donald Rapp and Paula Englander-Golden. **Total Cross Sections for Ionization and Attachment in Gases by Electron Impact. I. Positive Ionization**. *The Journal of Chemical Physics*, **43**(5):1464, May 1965. 17

[15] Monochromatic Electron, Impact Gas, and Ion Source. **Towards a High Brightness , Monochromatic Electron Impact Gas Ion Source Stellingen Naar een Monochromatische Elektronimpact Gas-Ionenbron met Hoge Helderheid**. *Source*, 1996. 18

Appendix A

List of Aperture Sizes

A.1 Data Table for Aperture Sizes

	Distance/m	Distance^2/m^2	Diameter/m	Ro/m	B_r/ (A/m^2(rad)eV	Aperture		
ISTB RF	0.45	0.2025	5.00E-04	2.50E-04	1.58	0.50	mm	
Chip								
Aperture for varying brightness	0.001	0.000001	2.252E-05	1.126E-05	1.58	22.52	μm	
with 1200eV energy	0.001	0.000001	1.128E-05	5.642E-06	25.00	11.28	μm	
and 300pA beam current	0.001	0.000001	9.489E-06	4.744E-06	50.00	9.49	μm	Maximum Current
	0.001	0.000001	7.979E-06	3.989E-06	100.00	7.98	μm	
	0.001	0.000001	5.642E-06	2.821E-06	400.00	5.64	μm	
	0.001	0.000001	4.744E-06	2.372E-06	800.00	4.74	μm	
	0.001	0.000001	4.487E-06	2.243E-06	1000.00	4.49	μm	
Aperture for varying brightness	0.001	0.000001	4.191E-05	2.096E-05	1.58	41.91	μm	
with 100eV energy	0.001	0.000001	2.100E-05	1.050E-05	25.00	21.00	μm	
and 300pA beam current	0.001	0.000001	1.766E-05	8.830E-06	50.00	17.66	μm	Maximum Current
	0.001	0.000001	1.485E-05	7.425E-06	100.00	14.85	μm	
	0.001	0.000001	1.050E-05	5.250E-06	400.00	10.50	μm	
	0.001	0.000001	8.830E-06	4.415E-06	800.00	8.83	μm	
	0.001	0.000001	8.351E-06	4.176E-06	1000.00	8.35	μm	
	Distance/m	Distance^2/m^2	Diameter/m	Ro/m	B_r/ (A/m^2(rad)eV	Aperture		
Aperture for varying brightness	0.001	0.000001	1.506E-05	7.530E-06	1.58	15.06	μm	
with 1200eV energy	0.001	0.000001	7.979E-06	3.989E-06	20.00	7.98	μm	
and 60pA beam current	0.001	0.000001	6.709E-06	3.355E-06	40.00	6.71	μm	
	0.001	0.000001	5.336E-06	2.668E-06	100.00	5.34	μm	20% of total current
	0.001	0.000001	4.487E-06	2.243E-06	200.00	4.49	μm	
	0.001	0.000001	3.773E-06	1.887E-06	400.00	3.77	μm	
	0.001	0.000001	3.409E-06	1.705E-06	600.00	3.41	μm	
	0.001	0.000001	3.173E-06	1.586E-06	800.00	3.17	μm	
	0.001	0.000001	3.001E-06	1.500E-06	1000.00	3.00	μm	
Aperture for varying brightness	0.001	0.000001	2.801E-05	1.401E-05	1.58	28.01	μm	
with 100eV energy	0.001	0.000001	1.485E-05	7.425E-06	20.00	14.85	μm	
and 60pA beam current	0.001	0.000001	1.249E-05	6.244E-06	40.00	12.49	μm	
	0.001	0.000001	9.931E-06	4.966E-06	100.00	9.93	μm	20% of total current
	0.001	0.000001	8.351E-06	4.176E-06	200.00	8.35	μm	
	0.001	0.000001	7.022E-06	3.511E-06	400.00	7.02	μm	
	0.001	0.000001	6.345E-06	3.173E-06	600.00	6.35	μm	
	0.001	0.000001	5.905E-06	2.953E-06	800.00	5.91	μm	
	0.001	0.000001	5.585E-06	2.792E-06	1000.00	5.58	μm	

	Ao=As/m²	A²/m⁴	Solid Angle	I/A	E/eV	B_r/ (A/m²(rad)eV	Aperture		
ISTB RF	1.96E-07	3.86E-14	9.70E-07	3.00E-10	1000	1.58	0.50	mm	
Chip				3.00E-10	30				
Aperture for varying brightness	3.983E-10	1.586E-19	3.98E-04	3.00E-10	1200	1.58	22.52	µm	
with 1200eV energy	1.000E-10	1.000E-20	1.00E-04	3.00E-10	1200	25.00	11.28	µm	
and 300pA beam current	7.071E-11	5.000E-21	7.07E-05	3.00E-10	1200	50.00	9.49	µm	Maximum
	5.000E-11	2.500E-21	5.00E-05	3.00E-10	1200	100.00	7.98	µm	Current
	2.500E-11	6.250E-22	2.50E-05	3.00E-10	1200	400.00	5.64	µm	
	1.768E-11	3.125E-22	1.77E-05	3.00E-10	1200	800.00	4.74	µm	
	1.581E-11	2.500E-22	1.58E-05	3.00E-10	1200	1000.00	4.49	µm	
Aperture for varying brightness	1.380E-09	1.904E-18	1.38E-03	3.00E-10	100	1.58	41.91	µm	
with 100eV energy	3.464E-10	1.200E-19	3.46E-04	3.00E-10	100	25.00	21.00	µm	
and 300pA beam current	2.449E-10	6.000E-20	2.45E-04	3.00E-10	100	50.00	17.66	µm	Maximum
	1.732E-10	3.000E-20	1.73E-04	3.00E-10	100	100.00	14.85	µm	Current
	8.660E-11	7.500E-21	8.66E-05	3.00E-10	100	400.00	10.50	µm	
	6.124E-11	3.750E-21	6.12E-05	3.00E-10	100	800.00	8.83	µm	
	5.477E-11	3.000E-21	5.48E-05	3.00E-10	100	1000.00	8.35	µm	
	Ao=As/m²	A²/m⁴	Solid Angle	I/A	E/eV	B_r/ (A/m²(rad)eV	Aperture		
Aperture for varying brightness	1.781E-10	3.173E-20	1.78E-04	6.00E-11	1200	1.58	15.06	µm	
with 1200eV energy	5.000E-11	2.500E-21	5.00E-05	6.00E-11	1200	20.00	7.98	µm	
and 60pA beam current	3.536E-11	1.250E-21	3.54E-05	6.00E-11	1200	40.00	6.71	µm	
	2.236E-11	5.000E-22	2.24E-05	6.00E-11	1200	100.00	5.34	µm	
	1.581E-11	2.500E-22	1.58E-05	6.00E-11	1200	200.00	4.49	µm	20% of total
	1.118E-11	1.250E-22	1.12E-05	6.00E-11	1200	400.00	3.77	µm	current
	9.129E-12	8.333E-23	9.13E-06	6.00E-11	1200	600.00	3.41	µm	
	7.906E-12	6.250E-23	7.91E-06	6.00E-11	1200	800.00	3.17	µm	
	7.071E-12	5.000E-23	7.07E-06	6.00E-11	1200	1000.00	3.00	µm	
Aperture for varying brightness	6.162E-10	3.797E-19	6.16E-04	6.00E-11	100	1.58	28.01	µm	
with 100eV energy	1.732E-10	3.000E-20	1.73E-04	6.00E-11	100	20.00	14.85	µm	
and 60pA beam current	1.225E-10	1.500E-20	1.22E-04	6.00E-11	100	40.00	12.49	µm	
	7.746E-11	6.000E-21	7.75E-05	6.00E-11	100	100.00	9.93	µm	
	5.477E-11	3.000E-21	5.48E-05	6.00E-11	100	200.00	8.35	µm	20% of total
	3.873E-11	1.500E-21	3.87E-05	6.00E-11	100	400.00	7.02	µm	current
	3.162E-11	1.000E-21	3.16E-05	6.00E-11	100	600.00	6.35	µm	
	2.739E-11	7.500E-22	2.74E-05	6.00E-11	100	800.00	5.91	µm	
	2.449E-11	6.000E-22	2.45E-05	6.00E-11	100	1000.00	5.58	µm	

	Distance/m	$Distance^2/m^2$	Diameter/m	Ro/m	B_r/ (A/m^2(rad)eV)	Aperture		
Aperture for varying brightness	0.001	0.000001	1.266E-05	6.332E-06	1.58	12.66	µm	10% of total current
with 1200eV energy	0.001	0.000001	6.709E-06	3.355E-06	20.00	6.71	µm	
and 30pA beam current	0.001	0.000001	5.642E-06	2.821E-06	40.00	5.64	µm	
	0.001	0.000001	4.487E-06	2.243E-06	100.00	4.49	µm	
	0.001	0.000001	3.773E-06	1.887E-06	200.00	3.77	µm	
	0.001	0.000001	3.173E-06	1.586E-06	400.00	3.17	µm	
	0.001	0.000001	2.867E-06	1.433E-06	600.00	2.87	µm	
	0.001	0.000001	2.668E-06	1.334E-06	800.00	2.67	µm	
	0.001	0.000001	2.523E-06	1.262E-06	1000.00	2.52	µm	
Aperture for varying brightness	0.001	0.000001	2.355E-05	1.178E-05	1.58	23.55	µm	10% of total current
with 100eV energy	0.001	0.000001	1.249E-05	6.244E-06	20.00	12.49	µm	
and 30pA beam current	0.001	0.000001	1.050E-05	5.250E-06	40.00	10.50	µm	
	0.001	0.000001	8.351E-06	4.176E-06	100.00	8.35	µm	
	0.001	0.000001	7.022E-06	3.511E-06	200.00	7.02	µm	
	0.001	0.000001	5.905E-06	2.953E-06	400.00	5.91	µm	
	0.001	0.000001	5.336E-06	2.668E-06	600.00	5.34	µm	
	0.001	0.000001	4.966E-06	2.483E-06	800.00	4.97	µm	
	0.001	0.000001	4.696E-06	2.348E-06	1000.00	4.70	µm	
	Distance/m	$Distance^2/m^2$	Diameter/m	Ro/m	B_r/ (A/m^2(rad)eV)	Aperture		
Aperture for varying brightness	0.001	0.000001	1.065E-05	5.325E-06	1.58	10.65	µm	5% of total current
with 1200eV energy	0.001	0.000001	5.642E-06	2.821E-06	20.00	5.64	µm	
and 15pA beam current	0.001	0.000001	4.744E-06	2.372E-06	40.00	4.74	µm	
	0.001	0.000001	3.773E-06	1.887E-06	100.00	3.77	µm	
	0.001	0.000001	3.173E-06	1.586E-06	200.00	3.17	µm	
	0.001	0.000001	2.668E-06	1.334E-06	400.00	2.67	µm	
	0.001	0.000001	2.411E-06	1.205E-06	600.00	2.41	µm	
	0.001	0.000001	2.243E-06	1.122E-06	800.00	2.24	µm	
	0.001	0.000001	2.122E-06	1.061E-06	1000.00	2.12	µm	
Aperture for varying brightness	0.001	0.000001	1.981E-05	9.904E-06	1.58	19.81	µm	5% of total current
with 100eV energy	0.001	0.000001	1.050E-05	5.250E-06	20.00	10.50	µm	
and 15pA beam current	0.001	0.000001	8.830E-06	4.415E-06	40.00	8.83	µm	
	0.001	0.000001	7.022E-06	3.511E-06	100.00	7.02	µm	
	0.001	0.000001	5.905E-06	2.953E-06	200.00	5.91	µm	
	0.001	0.000001	4.966E-06	2.483E-06	400.00	4.97	µm	
	0.001	0.000001	4.487E-06	2.243E-06	600.00	4.49	µm	
	0.001	0.000001	4.176E-06	2.088E-06	800.00	4.18	µm	
	0.001	0.000001	3.949E-06	1.974E-06	1000.00	3.95	µm	

	Ao=As/m^2	A^2/m^4	Solid Angle	I/A	E/eV	B_r/ (A/m^2(rad)eV	Aperture		
Aperture for varying brightness	1.260E-10	1.586E-20	1.26E-04	3.00E-11	1200	1.58	12.66	µm	10% of total current
with 1200eV energy	3.536E-11	1.250E-21	3.54E-05	3.00E-11	1200	20.00	6.71	µm	
and 30pA beam current	2.500E-11	6.250E-22	2.50E-05	3.00E-11	1200	40.00	5.64	µm	
	1.581E-11	2.500E-22	1.58E-05	3.00E-11	1200	100.00	4.49	µm	
	1.118E-11	1.250E-22	1.12E-05	3.00E-11	1200	200.00	3.77	µm	
	7.906E-12	6.250E-23	7.91E-06	3.00E-11	1200	400.00	3.17	µm	
	6.455E-12	4.167E-23	6.45E-06	3.00E-11	1200	600.00	2.87	µm	
	5.590E-12	3.125E-23	5.59E-06	3.00E-11	1200	800.00	2.67	µm	
	5.000E-12	2.500E-23	5.00E-06	3.00E-11	1200	1000.00	2.52	µm	
Aperture for varying brightness	4.357E-10	1.899E-19	4.36E-04	3.00E-11	100	1.58	23.55	µm	10% of total current
with 100eV energy	1.225E-10	1.500E-20	1.22E-04	3.00E-11	100	20.00	12.49	µm	
and 30pA beam current	8.660E-11	7.500E-21	8.66E-05	3.00E-11	100	40.00	10.50	µm	
	5.477E-11	3.000E-21	5.48E-05	3.00E-11	100	100.00	8.35	µm	
	3.873E-11	1.500E-21	3.87E-05	3.00E-11	100	200.00	7.02	µm	
	2.739E-11	7.500E-22	2.74E-05	3.00E-11	100	400.00	5.91	µm	
	2.236E-11	5.000E-22	2.24E-05	3.00E-11	100	600.00	5.34	µm	
	1.936E-11	3.750E-22	1.94E-05	3.00E-11	100	800.00	4.97	µm	
	1.732E-11	3.000E-22	1.73E-05	3.00E-11	100	1000.00	4.70	µm	
	Ao=As/m^2	A^2/m^4	Solid Angle	I/A	E/eV	B_r/ (A/m^2(rad)eV	Aperture		
Aperture for varying brightness	8.906E-11	7.932E-21	8.91E-05	1.50E-11	1200	1.58	10.65	µm	5% of total current
with 1200eV energy	2.500E-11	6.250E-22	2.50E-05	1.50E-11	1200	20.00	5.64	µm	
and 15pA beam current	1.768E-11	3.125E-22	1.77E-05	1.50E-11	1200	40.00	4.74	µm	
	1.118E-11	1.250E-22	1.12E-05	1.50E-11	1200	100.00	3.77	µm	
	7.906E-12	6.250E-23	7.91E-06	1.50E-11	1200	200.00	3.17	µm	
	5.590E-12	3.125E-23	5.59E-06	1.50E-11	1200	400.00	2.67	µm	
	4.564E-12	2.083E-23	4.56E-06	1.50E-11	1200	600.00	2.41	µm	
	3.953E-12	1.563E-23	3.95E-06	1.50E-11	1200	800.00	2.24	µm	
	3.536E-12	1.250E-23	3.54E-06	1.50E-11	1200	1000.00	2.12	µm	
Aperture for varying brightness	3.081E-10	9.494E-20	3.08E-04	1.50E-11	100	1.58	19.81	µm	5% of total current
with 100eV energy	8.660E-11	7.500E-21	8.66E-05	1.50E-11	100	20.00	10.50	µm	
and 15pA beam current	6.124E-11	3.750E-21	6.12E-05	1.50E-11	100	40.00	8.83	µm	
	3.873E-11	1.500E-21	3.87E-05	1.50E-11	100	100.00	7.02	µm	
	2.739E-11	7.500E-22	2.74E-05	1.50E-11	100	200.00	5.91	µm	
	1.936E-11	3.750E-22	1.94E-05	1.50E-11	100	400.00	4.97	µm	
	1.581E-11	2.500E-22	1.58E-05	1.50E-11	100	600.00	4.49	µm	
	1.369E-11	1.875E-22	1.37E-05	1.50E-11	100	800.00	4.18	µm	
	1.225E-11	1.500E-22	1.22E-05	1.50E-11	100	1000.00	3.95	µm	

A. LIST OF APERTURE SIZES

	Distance/m	$Distance^2/m^2$	Diameter/m	Ro/m	B_r/ $(A/m^2(rad)eV$	Aperture		
Aperture for varying brightness	0.001	0.000001	8.469E-06	4.234E-06	1.58	8.47	µm	
with 1200eV energy	0.001	0.000001	4.487E-06	2.243E-06	20.00	4.49	µm	
and 6pA beam current	0.001	0.000001	3.773E-06	1.887E-06	40.00	3.77	µm	
	0.001	0.000001	3.001E-06	1.500E-06	100.00	3.00	µm	2% of total current
	0.001	0.000001	2.523E-06	1.262E-06	200.00	2.52	µm	
	0.001	0.000001	2.122E-06	1.061E-06	400.00	2.12	µm	
	0.001	0.000001	1.917E-06	9.586E-07	600.00	1.92	µm	
	0.001	0.000001	1.784E-06	8.921E-07	800.00	1.78	µm	
	0.001	0.000001	1.687E-06	8.437E-07	1000.00	1.69	µm	
Aperture for varying brightness	0.001	0.000001	1.576E-05	7.881E-06	1.58	15.76	µm	
with 100eV energy	0.001	0.000001	8.351E-06	4.176E-06	20.00	8.35	µm	
and 6pA beam current	0.001	0.000001	7.022E-06	3.511E-06	40.00	7.02	µm	
	0.001	0.000001	5.585E-06	2.792E-06	100.00	5.58	µm	2% of total current
	0.001	0.000001	4.696E-06	2.348E-06	200.00	4.70	µm	
	0.001	0.000001	3.949E-06	1.974E-06	400.00	3.95	µm	
	0.001	0.000001	3.568E-06	1.784E-06	600.00	3.57	µm	
	0.001	0.000001	3.321E-06	1.660E-06	800.00	3.32	µm	
	0.001	0.000001	3.141E-06	1.570E-06	1000.00	3.14	µm	
	Distance/m	$Distance^2/m^2$	Diameter/m	Ro/m	B_r/ $(A/m^2(rad)eV$	Aperture		
Aperture for varying brightness	0.001	0.000001	5.411E-06	2.706E-06	1.58	5.41	µm	
with 1200eV energy	0.001	0.000001	3.409E-06	1.705E-06	10.00	3.41	µm	
and 1pA beam current	0.001	0.000001	2.711E-06	1.356E-06	25.00	2.71	µm	
	0.001	0.000001	2.411E-06	1.205E-06	40.00	2.41	µm	
	0.001	0.000001	1.997E-06	9.983E-07	85.00	2.00	µm	Smallest Current
	0.001	0.000001	1.612E-06	8.061E-07	200.00	1.61	µm	
	0.001	0.000001	1.402E-06	7.008E-07	350.00	1.40	µm	
	0.001	0.000001	1.225E-06	6.125E-07	600.00	1.22	µm	
	0.001	0.000001	1.123E-06	5.614E-07	850.00	1.12	µm	
	0.001	0.000001	1.078E-06	5.391E-07	1000.00	1.08	µm	
Aperture for varying brightness	0.001	0.000001	1.007E-05	5.036E-06	1.58	10.07	µm	
with 100eV energy	0.001	0.000001	3.409E-06	1.705E-06	10.00	3.41	µm	
and 1pA beam current	0.001	0.000001	2.711E-06	1.356E-06	25.00	2.71	µm	
	0.001	0.000001	2.411E-06	1.205E-06	40.00	2.41	µm	
	0.001	0.000001	1.997E-06	9.983E-07	85.00	2.00	µm	Smallest Current
	0.001	0.000001	1.612E-06	8.061E-07	200.00	1.61	µm	
	0.001	0.000001	1.402E-06	7.008E-07	350.00	1.40	µm	
	0.001	0.000001	1.225E-06	6.125E-07	600.00	1.22	µm	
	0.001	0.000001	1.123E-06	5.614E-07	850.00	1.12	µm	
	0.001	0.000001	1.078E-06	5.391E-07	1000.00	1.08	µm	

	Ao=As/m^2	A^2/m^4	Solid Angle	I/A	E/eV	B$_r$/ (A/m^2(rad)eV	Aperture		
Aperture for varying brightness	5.633E-11	3.173E-21	5.63E-05	6.00E-12	1200	1.58	8.47	µm	
with 1200eV energy	1.581E-11	2.500E-22	1.58E-05	6.00E-12	1200	20.00	4.49	µm	
and 6pA beam current	1.118E-11	1.250E-22	1.12E-05	6.00E-12	1200	40.00	3.77	µm	
	7.071E-12	5.000E-23	7.07E-06	6.00E-12	1200	100.00	3.00	µm	2% of total current
	5.000E-12	2.500E-23	5.00E-06	6.00E-12	1200	200.00	2.52	µm	
	3.536E-12	1.250E-23	3.54E-06	6.00E-12	1200	400.00	2.12	µm	
	2.887E-12	8.333E-24	2.89E-06	6.00E-12	1200	600.00	1.92	µm	
	2.500E-12	6.250E-24	2.50E-06	6.00E-12	1200	800.00	1.78	µm	
	2.236E-12	5.000E-24	2.24E-06	6.00E-12	1200	1000.00	1.69	µm	
Aperture for varying brightness	1.951E-10	3.807E-20	1.95E-04	6.00E-12	100	1.58	15.76	µm	
with 100eV energy	5.477E-11	3.000E-21	5.48E-05	6.00E-12	100	20.00	8.35	µm	
and 6pA beam current	3.873E-11	1.500E-21	3.87E-05	6.00E-12	100	40.00	7.02	µm	
	2.449E-11	6.000E-22	2.45E-05	6.00E-12	100	100.00	5.58	µm	2% of total current
	1.732E-11	3.000E-22	1.73E-05	6.00E-12	100	200.00	4.70	µm	
	1.225E-11	1.500E-22	1.22E-05	6.00E-12	100	400.00	3.95	µm	
	1.000E-11	1.000E-22	1.00E-05	6.00E-12	100	600.00	3.57	µm	
	8.660E-12	7.500E-23	8.66E-06	6.00E-12	100	800.00	3.32	µm	
	7.746E-12	6.000E-23	7.75E-06	6.00E-12	100	1000.00	3.14	µm	
	Ao=As/m^2	A^2/m^4	Solid Angle	I/A	E/eV	B$_r$/ (A/m^2(rad)eV	Aperture		
Aperture for varying brightness	2.300E-11	5.288E-22	2.30E-05	1.00E-12	1200	1.58	5.41	µm	
with 1200eV energy	9.129E-12	8.333E-23	9.13E-06	1.00E-12	1200	10.00	3.41	µm	
and 1pA beam current	5.774E-12	3.333E-23	5.77E-06	1.00E-12	1200	25.00	2.71	µm	
	4.564E-12	2.083E-23	4.56E-06	1.00E-12	1200	40.00	2.41	µm	
	3.131E-12	9.804E-24	3.13E-06	1.00E-12	1200	85.00	2.00	µm	Smallest Current
	2.041E-12	4.167E-24	2.04E-06	1.00E-12	1200	200.00	1.61	µm	
	1.543E-12	2.381E-24	1.54E-06	1.00E-12	1200	350.00	1.40	µm	
	1.179E-12	1.389E-24	1.18E-06	1.00E-12	1200	600.00	1.22	µm	
	9.901E-13	9.804E-25	9.90E-07	1.00E-12	1200	850.00	1.12	µm	
	9.129E-13	8.333E-25	9.13E-07	1.00E-12	1200	1000.00	1.08	µm	
Aperture for varying brightness	7.966E-11	6.346E-21	7.97E-05	1.00E-12	100	1.58	10.07	µm	
with 100eV energy	9.129E-12	8.333E-23	9.13E-06	1.00E-12	1200	10.00	3.41	µm	
and 1pA beam current	5.774E-12	3.333E-23	5.77E-06	1.00E-12	1200	25.00	2.71	µm	
	4.564E-12	2.083E-23	4.56E-06	1.00E-12	1200	40.00	2.41	µm	
	3.131E-12	9.804E-24	3.13E-06	1.00E-12	1200	85.00	2.00	µm	Smallest Current
	2.041E-12	4.167E-24	2.04E-06	1.00E-12	1200	200.00	1.61	µm	
	1.543E-12	2.381E-24	1.54E-06	1.00E-12	1200	350.00	1.40	µm	
	1.179E-12	1.389E-24	1.18E-06	1.00E-12	1200	600.00	1.22	µm	
	9.901E-13	9.804E-25	9.90E-07	1.00E-12	1200	850.00	1.12	µm	
	9.129E-13	8.333E-25	9.13E-07	1.00E-12	1200	1000.00	1.08	µm	